Journal of Applied Pharmaceutical Research
Volume 13 Issue 5, Year of Publication 2025, Page 91 – 113
DOI: https://doi.org/10.69857/joapr.v13i5.1176

Check for updates

Research Article

JOURNAL OF APPLIED PHARMACEUTICAL RESEARCH | JOAPR
www.japtronline.com ***ISSN: 2348 – 0335***

DESIGN AND OPTIMIZATION OF FOLATE-TARGETED LIPID-POLYMER HYBRID NANOPARTICLES CO-ENCAPSULATING DEXAMETHASONE AND CURCUMIN FOR SYNERGISTIC ANTI-INFLAMMATORY EFFICACY IN RHEUMATOID ARTHRITIS

Ekta Panchal[1,2], Shiv Kumar Yadav[2], Neha Jain[1], Mahima Chauhan[3], Archana Sharma[1]*

Article Information
Received: 14th May 2025
Revised: 25th August 2025
Accepted: 21st September 2025
Published: 31st October 2025

Keywords
Rheumatoid Arthritis, Folate-targeted Lipid-polymer hybrid nanoparticles, Dexamethasone, Curcumin, Nanocarrier optimization, Box Behnken Design, RAW 264.7 macrophage cells.

ABSTRACT
Background: Rheumatoid Arthritis (RA) is a chronic immune-mediated disorder characterized by synovial inflammation and joint destruction. Current therapies are limited by systemic toxicity and poor bioavailability. This research developed Dexamethasone (Dex) and Curcumin (Cur) loaded Folate Lipid Polymer Hybrid Nanoparticles (DCFLPs) to achieve synergistic anti-inflammatory action for RA. **Methodology:** DCFLPs were synthesized by the ionic gelation technique. Furthermore, Box-Behnken Design (BBD) formulations were optimized and evaluated for size distribution, PDI, ζ potential, structural features, % encapsulation efficiency (EE), in vitro release profile, and cell line studies using RAW 264.7 cells. **Results and Discussion:** Optimized DCFLPs revealed an average particle size of 287.8 ± 1.32 nm and PDI 0.25 with positive ζ potential 5.4 mV, and have shown high entrapment efficiencies for Dex (89.12 ± 0.087%) and Cur (98.27± 0.110%). Cytotoxicity assays showed superior anti-inflammatory activity, and enhanced cellular uptake was observed in cell line studies. **Conclusion:** DCFLPs offer an auspicious approach for targeted RA therapy by combining controlled drug release, reduced systemic toxicity, and enhanced site-specific delivery. These findings suggest that the synthesized formulation has the potential to serve as a viable approach for in vivo translation, future preclinical evaluation, and effective progression towards clinical application in RA management.

INTRODUCTION

Rheumatoid Arthritis (RA) is a persistent immune dysregulation condition characterized by symmetrical joint irritation, cartilage degradation**,** bone erosion**,** and synovial hyperplasia. Over time, RA may extend beyond the joints, affecting vital organs, lungs, kidneys, skin, heart, and eyes, and often results in functional impairment and reduced mobility [1]. Over the last few decades, the global burden of RA has increased markedly. Epidemiological data indicate a prevalence rate of 0.6% to 1% worldwide, with females three times as likely to be affected as

[1]*Amity Institute of Pharmacy, Amity University, Uttar Pradesh, Sector 125, Noida 201303, India.*
[2]*Anangpuria School of Pharmaceutical Sciences, Pt. B. D. Sharma University of Health Sciences, Alampur, Faridabad 121004, Haryana, India.*
[3]*HIMT College of Pharmacy, Greater Noida, Gautam Buddh Nagar, Uttar Pradesh 201310, India.*

For Correspondence: **asharma22@amity.edu**

males. Despite advances in therapeutic approaches, RA remains a substantial worldwide well-being challenge due to its unclear etiology & the lack of effective early diagnostic strategies [2]. Nanotechnology-based delivery systems offer key advantages over conventional therapies, including enhanced solubility, prolonged circulation time, targeted distribution, reduced systemic toxicity, and lower dosing frequency. These features collectively improve drug pharmacokinetics and pharmacodynamics. Currently, disease-modifying antirheumatic drugs (DMARDs), along with NSAIDs, glucocorticoids, and biologics, constitute the standard therapeutic approach for RA [3]. However, prolonged use of conventional therapies is associated with systemic side effects & suboptimal bio-distribution. To circumvent these challenges, targeted controlled-release systems offer a more effective alternative. Functionalization of drug molecules with targeting ligands enables active targeting, enhancing site-specific accumulation through interactions with macrophage surface receptors. This approach improves therapeutic efficacy and safety, representing a promising strategy for RA management [4,5]. Folic acid (FA) is vital for red blood cell formation, cell cycle progression, and nucleotide synthesis. Its small size and non-immunogenicity make it an ideal targeting ligand for drug delivery systems. Folate receptor (FR-β), which is overexpressed on activated macrophages, is a promising target in inflammatory diseases such as RA [6]. Activated macrophages overexpress folate receptor beta (FR-β), which binds folate-conjugated ligands. This binding facilitates receptor-mediated endocytosis, allowing selective internalization of the therapeutic payload into activated macrophages. This mechanism enhances targeted delivery while sparing healthy tissues [7]. Li et al. developed a folate-targeted nanoemulsion (MTX@PC-FA NE) encapsulating methotrexate, which preferentially accumulated in inflamed joints and macrophages in an AIA model, demonstrating improved therapeutic efficacy and reduced toxicity. These findings highlight the feasibility of folate-conjugated targeted nano-delivery platforms for macrophage modulation in RA [8]. Nasra et al. designed a folate-functionalized liposomal system for the delivery of methotrexate (MTX) and RELA siRNA, enabling targeted uptake by RAW264.7 macrophages. The system promoted M1-to-M2 polarization and demonstrated significant anti-arthritic efficacy in a CIA rat model, indicating its promise as a macrophage-targeted immunotherapeutic approach for RA [9]. Chitosan (Chi), a cationic polysaccharide derived from chitin deacetylation, exhibits pH-dependent electrostatic interactions with anionic biomolecules. It has biocompatibility, mucoadhesiveness, and the capacity to form nanoparticles; it serves as a cost-efficient, multifunctional platform for passive and active drug delivery. Chi-based nanocarriers are widely used to enhance drug stability, enable sustained and controlled release, and achieve targeted delivery in pharmaceutical and biomedical applications [10,11]. Al-Nemrawi et al. formulated Chi nanoparticles for MTX delivery via a transdermal route, demonstrating improved drug retention and synovial penetration by mitigating lipid peroxidation. Similarly, Naseer et al. prepared GEO-CNPs via ion-induced gelation and demonstrated restorative efficacy in an FCA-induced arthritic rat model [12].

Phospholipids are biocompatible, amphipathic, and facilitate the embedding of water-soluble and lipid-soluble drugs, making them promising for targeted delivery [13]. Peng X et al. established a BBR-loaded PPSG, demonstrating excellent stability and a significant decline in TNF-α levels in AIA rats & OIA rabbits. This study confirms that the phospholipid-based delivery system effectively targeted BBR, enabling successful treatment of RA [14]. However, phospholipid-based delivery systems offer good entrapment properties and controlled drug release for hydrophobic drugs. Still, challenges such as heterogeneous distribution, drug leakage, poor drug encapsulation, and short shelf life persist for hydrophilic drugs, limiting the widespread application of lipid-based nanoparticles. In contrast, polymeric nanoparticle delivery systems offer various advantages but also have drawbacks, such as rapid elimination from the body, a detrimental impact of the organic solvents used during synthesis, low drug-loading efficacy, and a high-cost fabrication process, which curtails their use. These disadvantages associated with both delivery systems can be overcome by using Lipid–polymer hybrid nanoparticles (LPHNPs) [15]. LPHNPs have emerged as a promising delivery system that combines the features of both liposomes and polymer-based systems and also overcomes their limitations through their core-shell hybrid nanostructure. Various studies have reported numerous benefits of LPHNPs, including enhanced stability, increased drug-loading efficacy, higher encapsulation efficiency, a good biocompatibility profile, and reduced drug leakage. In addition, surface modification/ functionalization with an appropriate ligand also improved the targeting ability and site specificity of these hybrid nanoparticles. Zhang J et al. developed dextran sulfate-modified paeoniflorin pH-responsive LPHNPs (Pae–PPNPs–DS) for the

treatment of RA. Their results confirm that Pae–PPNPs–DS showed good cellular uptake in RAW 264.7 macrophage cell lines, modulated the STAT signaling pathway, successfully inhibited pro-inflammatory and M1 markers, and mimicked anti-inflammatory action and M2 marker secretion [16]. Dexamethasone (Dex), a glucocorticosteroid with anti-inflammatory and immunosuppressive properties, has long been a first-line treatment for RA. Zhang et al. revealed that Dex palmitate-loaded modified human serum albumin nanoparticles target the scavenger receptor A on activated macrophages in LPS-activated RAW264.7 cells. Moreover, Kim et al. prepared dexamethasone-loaded RMSNs, achieving 92% sustained release and enhanced in vivo efficacy in RA [17, 18]. Curcumin (Cur), a hydrophobic polyphenol, is widely used in nanodrug delivery owing to its strong antioxidant, Anti-Inflammatory, antimicrobial, anti-rheumatic, & Antineoplastic activities. These therapeutic effects are mainly linked to the suppression of pro-inflammatory signaling factors, comprising IL-6, TNF-α, IL-1β, & COX-2, predominantly secreted by activated macrophages [19]. Asif HM et al. developed chitosan-STPP nanoparticles to enhance Cur bioavailability, achieving entrapment efficiencies of approximately 65% and anti-inflammatory activity of approximately 75% via the HRB membrane stabilization assay. Similarly, Aslam B et al. designed PLGA nanoparticles co-loaded with Cur and meloxicam to evaluate the therapeutic efficacy against arthritis in CFA-induced rat models [20, 21].

In the literature, Cur has well-documented anti-inflammatory and antioxidant properties and has revealed clinical benefit in RA patients, improving inflammatory biomarkers and clinical scores in meta-analyses [22]. Yan F et al. combined curcumin with low doses of glucocorticoids, such as prednisolone, and found that this combination substantially enhanced anti-arthritic efficacy while mitigating steroid-induced toxicity in Freund's adjuvant-induced arthritis in rats, demonstrating synergistic inhibition of pro-inflammatory cytokines and reduced adverse effects. Nanoparticle co-delivery of prednisolone and curcumin in human serum albumin nanoparticles provided a superior therapeutic effect compared with single-drug or free combinations in adjuvant-induced arthritis models, due to enhanced joint targeting and synchronized drug release [23].

The tailored nature of these nanoparticle formulations promotes the accumulation of the therapeutic agent at the targeted site and boosts therapeutic efficacy. This novel, synergistic strategy overcomes the limitations of conventional therapy, thereby improving therapeutic outcomes.

MATERIALS AND METHODS

Materials

Dex and Cur (98% purity) were purchased from GLR Innovations, New Delhi, India. Soya lecithin was obtained from CDH, New Delhi, India. Medium MW chitosan with 90% degree of deacetylation and FA (pure, 98%) was sourced from SRL Pvt. Ltd., India. The RAW 264.7 cell line, derived from activated macrophages, was obtained from the National Center for Cell Sciences (NCCS), Pune, India. Ethanol & acetic acid are acquired from Fisher Scientific, India. The Rhodamine B dye was purchased from Sigma-Aldrich (St Louis, USA). The study employed solvents and chemicals of analytical grade purity, used as received.

Preformulation Studies

Preformulation studies were conducted to evaluate the physicochemical properties of Dex and Cur before the formulation of lipid-polymer hybrid nanoparticles. The organoleptic characteristics (color, odor, and form), melting point, determination of λ-max in UV-Vis spectrophotometry, and HPLC calibration curve development were determined. Their thermal and crystallographic properties, and the interaction between the drug and excipients (FA, chitosan, soya lecithin, and PVP), were investigated by FTIR, Differential Scanning Calorimetry (DSC), and X-ray Diffraction (XRD).

The absorbance of the drugs was determined using a UV-Vis spectrophotometer (Shimadzu UV-1800, Japan) by measuring the absorbance of standard solutions of Dex (40 µg/mL) and Cur (10 µg/mL) in methanol: water (2:1) at 200-400 nm. Calibration curves for both drugs (10-60 µg/mL) were generated via HPLC (Shimadzu Corp., Kyoto, Japan) after filtration through 0.22 µm membranes [22]. Subsequently, FTIR analysis was conducted on the pure drug compounds, drug-drug mixtures, and drug-excipient mixtures to evaluate compatibility. Physical mixtures (1:1 ratio) were stored at room temperature and analyzed after 15 days using an FTIR spectrophotometer (Bruker Alpha, Berlin, Germany). Samples (2-4 mg) were scanned in the 4000-400 cm^{-1} range to detect potential interactions.

HPLC Validation Method

A specific and reproducible reversed-phase (RP) HPLC method was developed for the simultaneous qualitative and quantitative

determination of Dex and Cur in a bulk mixture. HPLC system outfitted with a photodiode array (PDA) detector and a C18 analytical column (250 × 4.6 mm, 5 µm) maintained at 30 °C with 0.1% orthophosphoric acid and acetonitrile in a 30:70 (v/v) ratio of mobile phase, delivered at a flow rate of 1 mL/min. 10 µL injection volume and 280 nm wavelength were used. Method validation was performed in accordance with ICH guidelines, evaluating linearity, accuracy, precision, robustness, limit of detection (LOD), and limit of quantitation (LOQ) [24, 25].

Preparation of Folate- Chitosan (FA-Chi) Conjugates

The conjugation of FA to chitosan was achieved using a carbodiimide coupling reaction (Figure 1). In brief, 0.75 g of FA in 12.5 mL of dimethyl sulfoxide (DMSO) at ambient temperature; subsequently, 1.43 g (1.0 M) NHS, 2.58 g (1.0 M) DCC, and 1 mL triethylamine were mixed. The sample was sonicated and stirred in the dark for 17 hours, filtered to remove dicyclohexylurea, and washed with 30% acetone (3–4 times). For conjugation, 45 mg of chitosan was dispersed in an acetate buffer (pH 5.6), and NHS-activated FA in DMSO was incorporated. The chemical interaction was stirred at 30°C for 20 h in the dark at 2500 rpm, at pH 9.0 using 1 M NaOH. The sample was centrifuged at 6000 rpm for 15 minutes using a 10 kDa MWCO, then washed with DMSO to remove excess NHS ester, followed by deionized water, and lyophilized for 24 hours [26, 27].

Characterization of Synthesized FA-Chi Conjugates

Fourier Transform Infrared (FTIR) Spectroscopy

FTIR analysis was performed to detect and characterize the chemical moieties & assess potential physicochemical interactions among the formulation components. The spectra of FA, chitosan, and the FA–Chi conjugate were analyzed using a Bruker Alpha spectrometer (Spectrum Two, Berlin, Germany) with OPUS 5.5 software over the 4000–400 cm^{-1} range [28].

^{1}HNMR Spectroscopy

^{1}H NMR spectroscopy verifies the successful conjugation of FA-chitosan, employing a Bruker AV-500 MHz NMR spectrometer for spectral acquisition. FA was dissolved in DMSO-d_6, while chitosan & FA–Chi conjugates were solubilized in a deuterated acetic acid/deuterium oxide (CD_3COOD/D_2O) system. The spectra of each component were recorded and compared with those of the individual constituents to confirm successful conjugation through characteristic chemical shift changes associated with amide bond formation [29].

Design of Experiment (DoE) for Formulation Optimization

To optimize the FA-targeted DCFLP nanoparticles, Box-Behnken Design (BBD) was employed using Design-Expert Software (Version 8.0.4, Stat-Ease Inc., Minneapolis, MN. The design suggested 17 experimental runs with three independent variables: FA–Chi conjugates concentration (X_1), soya lecithin concentration (X_2), and homogenization speed (X_3). These independent variables were selected and finalized based on prior literature and initial trial studies [30]. Dependent variables included entrapment efficiency of Dex (Y_1), entrapment efficiency of Cur (Y_2), and particle size (Y_3). Each factor was evaluated at three levels, based on preliminary studies and literature. The objective was to maximize Y_1 and Y_2 while minimizing Y_3 (Table 1). The successive second-order polynomial equation sculpted the system response (Y):

$$Y = \beta_0 + \beta_1 X_1 + \beta_2 X_2 + \beta_3 X_3 + \beta_{11} X_1^2 + \beta_{22} X_2^2 + \beta_{33} X_3^2 + \beta_{12} X_1 X_2 + \beta_{13} X_1 X_3 + \beta_{23} X_2 X_3$$

Where, Y denotes the measured response of the dependent variables as influenced by varying levels of independent variables (X_1, X_2, X_3); β_0 is the intercept; $\beta_1, \beta_2, \beta_3$ are the linear regression coefficients; $\beta_{12}, \beta_{13}, \beta_{23}$ represent interaction terms; and $\beta_{11}, \beta_{22}, \beta_{33}$ denote quadratic coefficients, capturing the curvature effects of the formulation parameters [31]. The process parameters were optimized to achieve the desired responses, while all other variables (e.g., drug concentration, sonication amplitude, and temperature) were maintained constant to minimize experimental variability.

Preparation of FA-targeted Dex and Cur-loaded lipid-polymer hybrid nanoparticles

DCFLP were formulated through the ionic gelation method, which relies on electrostatic interactions between cationic chitosan and anionic soya lecithin at ambient temperature. Blank Folate Lipid Polymer Hybrid Nanoparticles (FLP) were synthesized by dissolving FA-Chi conjugates in 0.25% acetic acid to form the aqueous phase, while soya lecithin was solubilized in ethanol for the organic phase. Drop-wise phase transfer from the organic to the aqueous phase was performed under constant agitation at 10,000 rpm to facilitate emulsification, followed by homogenization for 15 min to achieve a clear dispersion. Drug-loaded nanoparticles were prepared similarly, incorporating Dex and Cur (1:1 molar ratio)

into the organic phase. Various formulations were developed by adjusting the concentrations of FA-Chi conjugates and soya lecithin to optimize particle size, surface charge, payload entrapment, and entrapment efficiency [32].

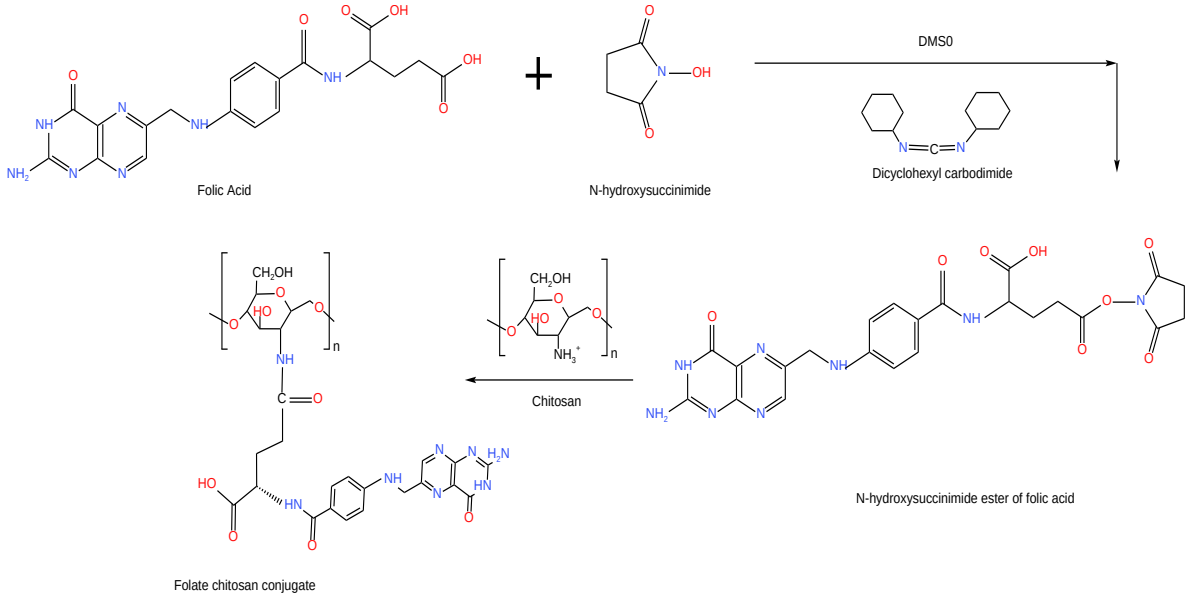

Figure 1: The chemical reaction representing the synthesis procedure of FA-Chi conjugate preparation

Table 1: Independent variables, Dependent variables, and Constraints for 3^3 Box-Behnken Design

LEVELS						
Independent variables				Low (-1)	Medium (0)	High (+1)
X_1= Amount of FA-Chi conjugates (mg)				10	55	100
X_2= Amount of Soya lecithin (mg)				10	30	50
X_3= Homogenization speed (rpm)				7500	10000	12500
Independent variables				**Dependent variables**		
	X_1	**X_2**	**X_3**	**Y_1= % Entrapment Dex**	**Y_2= % Entrapment Cur**	**Y_3= Particle size (nm)**
Constraints	In range	In range	Maximum	Maximum	Maximum	Minimum
Importance	+++	+++	+++	++++	++++	+++

Physical Appearance, % Entrapment Efficiency (% EE) and % Drug Loading (% DL)

The prepared DCFLP formulation was visually examined for its physical traits (e.g., color, size, and shape). Quantification of Dex and Cur in DCFLP nanoparticles was conducted using a Shimadzu 1800 UV-visible spectrophotometer at 280 nm. Briefly, the nanoparticle formulation (1:1 molar ratio) was dispersed in methanol & centrifugation was performed at 15,000 rpm for 15 minutes to isolate the desired particles. The upper layer of obtained liquid was filtered by a 0.45 µm membrane filter & interpreted by HPLC (Shimadzu Corp., Kyoto, Japan) to determine the amount of unencapsulated drug [33]. The % EE & % DL calculations were obtained using the following equations:

$$\textit{Percentage Entrapment Efficiency}\ (\%EE) = \frac{Dtotal - Dfree}{Dtotal} \times 100$$

Where, $Dtotal - Dfree$ *= the total drug content in the formulation,* $Dtotal$ *= the amount of unentrapped drug*

$$\textit{Percentage Drug Loading}\ (\%\ DL) = \frac{Dencap}{WNP} \times 100$$

Where, D_{encap}*= the amount of drug successfully encapsulated within the nanoparticles,* W_{NP} *= the weight of nanoparticles used*

Particle size, Polydispersity Index (PDI), and zeta potential

Hydrodynamic granule size, PDI, & ζ of blank FLP & DCFLP nanoparticles were analyzed using a Litesizer™ 500 (Anton Paar GmbH, Austria). Before measurement, each sample was diluted 50-fold with deionized water. Measurements were conducted at a wavelength of 658nm & a scattering angle of 165°. All values are stated as the mean of 3 independent measurements [34, 35].

Differential Scanning Calorimetry (DSC)

DSC was performed on pure Dex, Cur, and DCFLP nanoparticles using a DSC 6000 instrument to investigate the physicochemical interaction. In brief, 5 mg of sample was sealed in 40 µL aluminum pans & subjected to a thermal scan from 30 °C to 300 °C at 10°C/min under a nitrogen atmosphere (flow

rate: 20 mL/min). Pyris software was used to record the thermograms.

X-ray diffraction (XRD) analysis

XRD profiling was performed on a mixture of Dex, Cur, and DCFLP nanoparticles to evaluate the crystalline structures of the chemical compounds using an X-ray diffractometer. The X-ray diffraction (XRD) profiles were recorded using a powder X-ray diffractometer (Ultima-4, Rigaku Company, Japan) with CuKα radiation, a Kβ filter, an excitation voltage of 40 kV, and a tube current of 30 mA. Diffraction data were collected within a 2θ range of 10.00° to 60.00°. Additionally, diffractograms were attained up to a final angle of 50° with Cu Kα radiation & the angular increment of 0.02° [36].

Transmission Electron Microscopy (TEM)

The surface morphological images of blank FLP & drug-loaded DCFLP nanoparticles were evaluated using transmission electron microscopy (TEM). Each formulation was applied as a drop onto carbon-coated copper grids, air-dried & negatively stained with 2% w/v phosphotungstic acid for 1min. After appropriate drying at ambient temperature, the grids were observed under a TEM at 200 kV [37].

Determination of conjugation efficiency and folate content

The following formula determined the conjugation efficiency of the folate with chitosan:

$$\textbf{Conjugation Efficiency}\ (\%) = \frac{\textbf{Amount of folate conjugated}}{\textbf{Amount of folate initially taken}} \times 100$$

A microplate reader calculated the quantity of folate in the FA-Chi conjugated nanoparticles. Concisely, 200 µL of nanoparticles were freeze-dried and dissolved in DMSO: DCM (4:1). After 6 hrs of vortexing, the sample was centrifuged, and the collected supernatant was examined by UV-visible spectrophotometry at 364 nm. A standard calibration plot of folic acid was prepared for the determination of total folic acid content in the FA-Chi conjugated nanoparticles [34]. The given formula calculated the % of folate content:

$$\textit{Folate content}\ (\%) = \frac{\textit{Folate content within nanoparticle}}{\textit{Folate content added in nanoparticle}} \times 100$$

Drug release study

Drug liberation under simulated conditions of Dex and Cur was measured via the dialysis method. The dialysis membrane (1 kDa MWCO), which was pre-soaked in 40% ethanol overnight, was loaded further with 2 mL PBS (pH 7.4) containing nanoparticles corresponding to 50 mg of each drug. The sealed bag was immersed in 50 mL PBS & agitated at 100 rpm, 37 ± 0.5 °C. At the specific time points, 2 mL portions were sampled & replaced to maintain pseudo-sink conditions. The collected samples at specific time intervals were analyzed for the drug content of Dex and Cur in the optimized formulation by using the HPLC method. Drug release profiles were plotted for different samples and analyzed using various kinetic models [38, 39].

Stability studies as per ICH guidelines

Stability assessments are conducted in accordance with ICH regulatory guidelines. DCFLP nanoparticle formulations were stored at 4°C and room temperature for 180 days, with weekly monitoring for changes in micelle appearance. Hydrodynamic particle size (nm), PDI (%), EE (%), and ζ potential (mV) were evaluated at 0, 30, 90, and 180 days [40].

Cell Culture

RAW 264.7 cells were procured from the National Center for Cell Sciences (NCCS), Pune. RAW 264.7 cells were matured in the high-glucose Dulbecco's Modified Eagle's Medium (DMEM) with 10% Fetal Bovine Serum (FBS) and incubated at 37°C in a 5% CO_2 atmosphere.

Cytotoxicity Study

Cytotoxicity of DCFLP nanoparticles was evaluated in RAW 264.7 macrophage cells via the MTT assay. Cells were seeded at 1×10^4 per well in 96-well plates and activated with LPS (1 µg/mL). Cells were treated with varying concentrations. (5–100 µg/mL) of the DCFLP nanoparticle formulation for 24 hours. Following treatment, the medium was replaced with MTT solution (5 mg/mL in PBS, pH 6.8), and incubation continued for 2 hours. The supernatant was decanted, and the formazan crystals were suspended in 100 µL DMSO. Absorbance was recorded at 570 nm using an ELISA plate reader [41]. Cell viability (%) was calculated by using the following formula:

$$\textit{Cell viability}\ (\%) = \frac{\textit{Absorbance of treated cells}}{\textit{Absorbance of control cells}} \times 100$$

Intracellular uptake study

Intracellular uptake of DCFLP nanoparticles was assessed in RAW 264.7 cells, with Rhodamine B used as a fluorescent tracer. Cells were cultured in 12-well plates and incubated at 37°C for 24 hours under the specified culture conditions. After

that, cells were treated with Rhodamine B-loaded DCFLP nanoparticles at concentrations of 5 and 10 µg. After incubation, the cells were trypsinized and analyzed by fluorescence microscopy to assess the formulation's uptake [39].

Statistical analysis

All acquired results were assessed using the ANOVA model to measure the variance and identify the significant study of independent variables on the dependent variables, along with the characteristics of the developed nanoparticle formulation. The data were statistically represented as mean ± standard deviation (SD, n=3). The Design Expert Version 8.0.4 was employed for the analysis, with statistical significance evaluated at a 95% confidence interval level ($p < 0.05$) [44].

RESULT AND DISCUSSION

Preformulation studies

Dex and Cur appeared as doorless white and yellow powders, respectively. After thermal analysis, the melting point was determined to be 262.40 °C ± 0.563 to 263.06 °C ± 0.015 for Dex and 182.37 °C ± 0.561 to 183.04 °C ± 0.035 for Cur. The absorption maxima of Dex and Cur were recorded at 239 nm and 426 nm, respectively, with an isobestic point at 280 nm in the overlaid spectra shown in Figures 2(A), (B), and (C). Standard curves for both drugs (10–60 µg/ml) were constructed at 280 nm, yielding regression equations Y = 21177x – 6817 (R^2 = 0.999) for Dex and Y = 130237x – 30629 (R^2 = 0.999) for Cur, confirming excellent linearity as shown in Figures 3 (A), and (B). FTIR analysis of the drug-drug mixture (1:1) showed no significant interactions along with excipients, as mentioned in Table 2. These results validate the compound's suitability for further formulation and characterization [45].

HPLC Validation Method

The developed RP-HPLC method successfully separated Dex and Cur, with distinct peaks at 3.16 and 4.16 minutes, respectively. The method demonstrated acceptable system suitability and validation parameters. The sensitivities, as indicated by LOD and LOQ, were 0.232 µg/mL and 0.704 µg/mL for Dex, and 0.065 µg/mL and 0.198 µg/mL for Cur, respectively. The method exhibited good linearity, precision, and accuracy, confirming its suitability for simultaneous quantification of both drugs. These findings support its application in pharmaceutical formulations or research involving the combination of Dex and Cur [24,25].

FTIR Spectroscopy

The FTIR spectrum of chitosan (Figure 4A) displayed a prominent peak at 3339.26 cm^{-1}, corresponding to hydroxyl (−OH) and amino (−NH) group stretching vibrations. Peaks at 2930.04 and 2866.97 cm^{-1} were linked to symmetric and asymmetric C–H stretching, respectively. An absorption band at 1236.75 cm^{-1} indicated the glycosidic ring, while a peak at 1022.82 cm^{-1} confirmed carbonyl (C=O) stretching. The FTIR spectrum of pure FA (Figure 4B) showed peaks between 3450–3350 cm^{-1}, signifying carboxylic OH stretching of glutamic acid and N–H stretching of the pterin ring, with a distinct peak at 1690.93 cm^{-1} confirming carboxylic C=O stretching. The FA-Chi conjugate (Figure 4C) FTIR spectrum revealed a peak at 1623 cm^{-1}, indicating amide bond formation, while the disappearance of free amide group peaks and a new absorption band at 1014 cm^{-1} confirmed successful conjugation. These findings collectively validate the chemical derivatization of chitosan with folic acid [42].

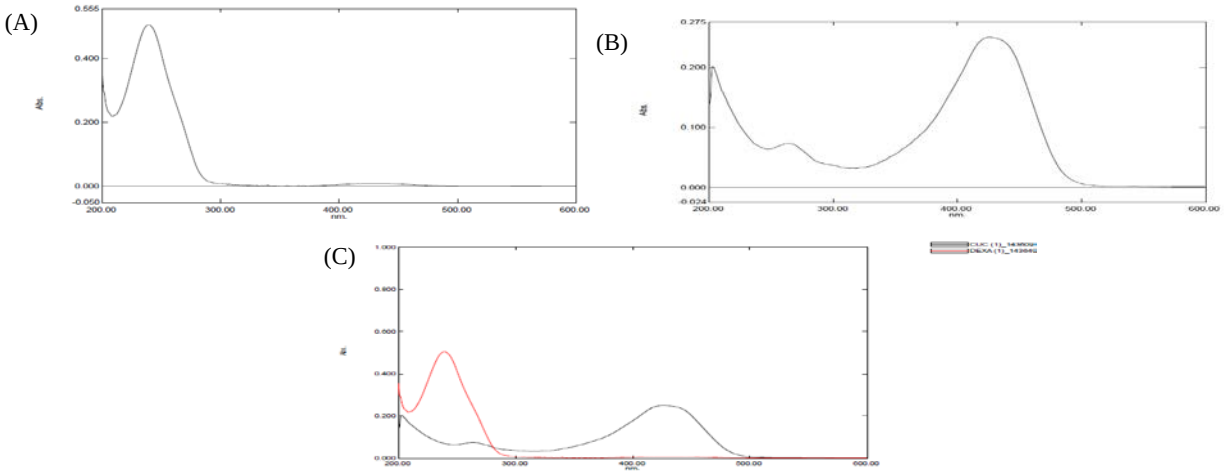

Figure 2: A) UV Spectrum of Dex showing absorption maxima at 239 nm B) UV Spectrum of Cur showing absorption maxima at 426 nm, C) Overlay UV Spectrum of Dex and Cur showing isobestic point at 280 nm

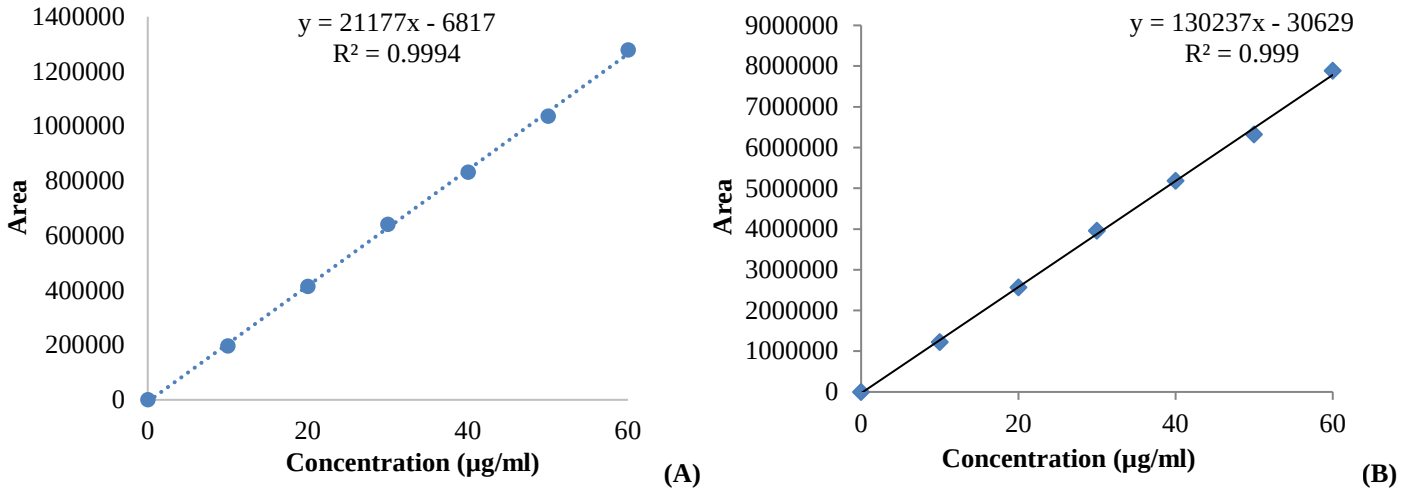

Figure 3: Standard calibration plot of A) Dex, B) Cur by RP-HPLC

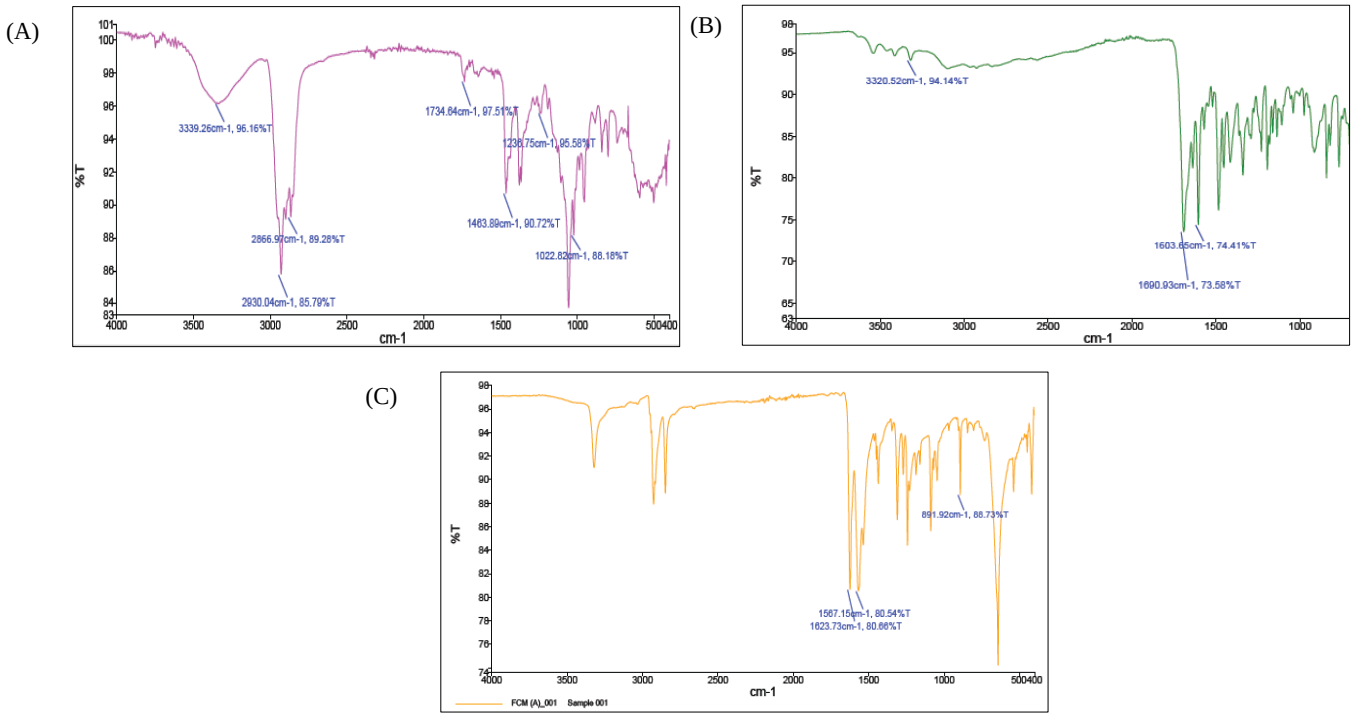

Figure 4: FT-IR spectral representation of (A) Chitosan (B) FA, (C) FA-Chi conjugates

Table 2: Compatibility studies of drugs and excipients using FTIR

Sr. No.	Frequency assignment	Wave number (cm^{-1})
Observed wavenumbers (cm^{-1}) of Dex		
1	O-H group	3388.52
2	C-H stretching vibration	2953.23
3	–C=N– stretching	1663.27
4	-C=O stretching	1621.32
5	C-F stretching	1268.84
Observed wavenumbers (cm^{-1}) of Cur		
6	Aromatic moiety C=C stretching	1626.99
7	Benzene ring stretching vibrations	1602.47
8	C=O and C=C vibrations	1506.04
9	Olefinic C-H bending vibrations	1427.79
10	Aromatic C-O Stretching Vibrations	1280.93
11	C-O-C stretching vibrations	1026.49

Observed wavenumbers (cm^{-1}) of Dex and Cur		
12	-C=O stretching	1708.82
13	-C=O stretching	1663.81
14	-C=O stretching	1622.23
15	Benzene ring stretching vibrations	1603.31
16	C=O and C=C vibrations	1508.02
17	Olefinic C-H bending vibrations	1428.51
18	Aromatic C-O Stretching Vibrations	1281.64
19	C-O-C stretching vibrations	1031.99
Observed wavenumbers (cm^{-1}) of drug-excipients physical mixture		
20	C-H stretching vibration	2948.15
21	C-F stretching	1262.67
22	C=O and C=C vibrations	1512.32

^{1}HNMR spectroscopy

^{1}H NMR spectra were employed to confirm the conjugation of FA-Chi. The spectrum of pure chitosan (Figure 5A) displayed a peak at 2.4942 ppm, corresponding to the methyl protons of the acetamino group (–CH_3), and another signal at 3.3519 ppm related to the –CH proton of the glucosamine unit. FA (Figure 5B) showed aromatic proton signals between 5.7–5.8 ppm, along with a singlet at 3.40 ppm attributed to a specific proton of FA. The ^{1}H NMR spectrum of the FA-Chi conjugate (Figure 5C) revealed a new peak at 2.5330 ppm, indicating successful amide bond formation between the activated ester of FA & the primary amine groups of chitosan, confirming the conjugation [43].

BBD for the optimization of Dex and Cur loaded FA-Chi conjugated lipid hybrid nanoparticle

In the present study, BBD was employed to evaluate the influence of three independent formulation variables on critical response parameters, as outlined in Table 1. Initially, the formulation variables and process variables were optimized based on particle size, PDI, and Dex-Cur percentage entrapment as shown in Tables 3 and 4. A design comprising 17 runs was implemented to investigate the effects on key formulation responses, including Dex entrapment (Y1), Cur entrapment (Y2), and particle size (Y3). Data interpretation was carried out using Design-Expert software (Version 7.1.6). A response surface methodology employing a quadratic model was applied, and statistical analysis was performed using ANOVA and R^2 metrics. Model significance was confirmed by p-values ($p < 0.005$), while the R^2 values-ideally approaching 1, were used to evaluate model fitness and variance explanation. Entrapment efficiency of Dex and Cur ranged from $66.220 \pm 0.557\%$ to $91.354 \pm 0.099\%$, and $94.166 \pm 0.189\%$ to $98.128 \pm 0.270\%$, respectively. Particle sizes among the formulations varied between 210.33 ± 1.527 nm and 895.33 ± 2.00 nm.

The quadratic model was found to provide the most suitable fit for the responses (i.e. Y1, Y2, & Y3) demonstrating statistical significance ($p < 0.005$). Furthermore, the difference between the adjusted R^2 and predicted R^2 values remained below 0.2 for all responses, indicating strong model predictability and consistent particle size distribution across the formulations [44].

Effect of independent variables on % entrapment of Dex

The data obtained for the predicted and observed responses of Y1 were evaluated based on the BBD. Various combinations of independent variables, FA-Chi concentration (X1), phospholipid amount (X2), and homogenization speed (X3) were selected, and their influence on the response Y1 was expressed through the following mathematical model:

$$\%\ \boldsymbol{Entrapment\ of\ Dex} = \mathbf{85.4676} + \mathbf{6.728625}.\boldsymbol{X1} + \mathbf{4.91325}.\boldsymbol{X2} + \mathbf{0.704125}.\boldsymbol{X3} + \mathbf{0.23075}.\boldsymbol{X1}.\boldsymbol{X2} - \mathbf{0.7665}.\boldsymbol{X1}.\boldsymbol{X3} - \mathbf{2.15275}.\boldsymbol{X2}.\boldsymbol{X3} + \mathbf{6.2008}.\boldsymbol{X1^2} - \mathbf{1.27005}.\boldsymbol{X2^2} + \mathbf{1.1032}.\boldsymbol{X3^2}$$

The impact of the selected independent variables (X1, X2, X3) and their interactions (X1·X2, X1·X3, X2·X3) was assessed using the quadratic model equation. The influence on the dependent variable, specifically the entrapment efficiency of Dex (Y1), was determined based on p-values and F-values. BBD incorporated a 3D response surface quadratic model to evaluate these effects.

Model significance was validated using R^2 and ANOVA (Table 6). The R^2, F-value, and p-value for Y1 were 1.132, 65.39, and <0.0001, respectively, confirming the substantial influence of independent variables on the predicted responses (Table 5). The 3D surface response graph for percentage entrapment of Dex (Y1) was depicted in Figures 6 (A), (B), & (C) [42].

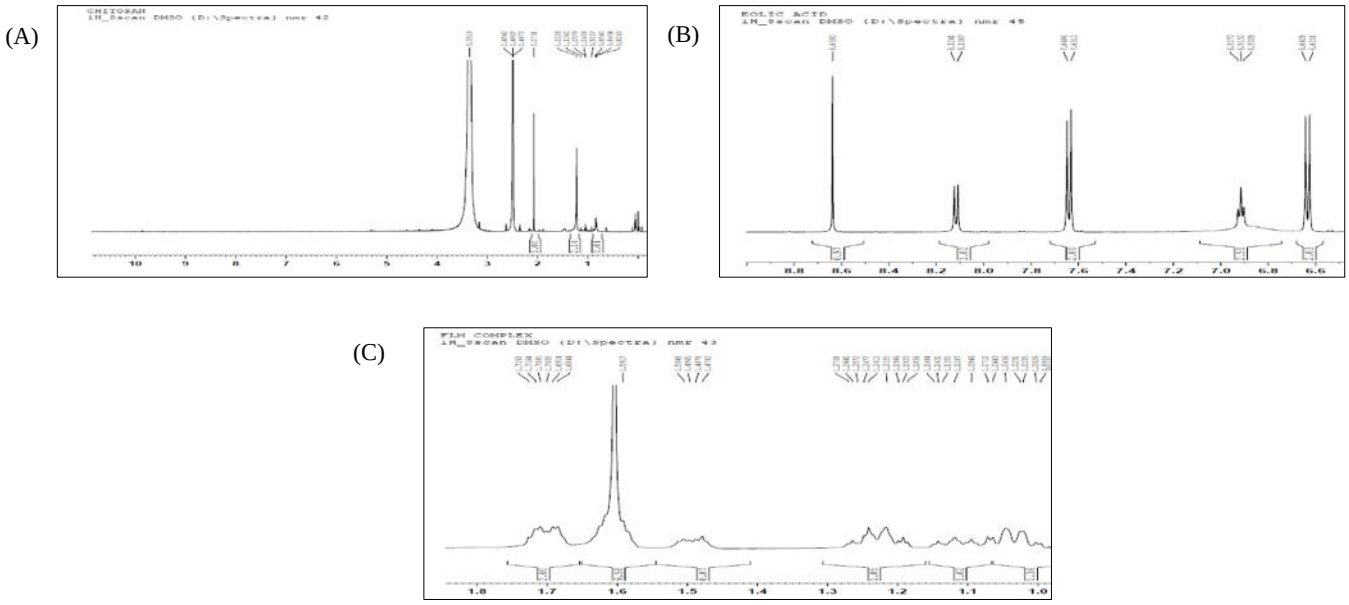

Figure 5: ^{1}H-NMR spectral representation of (A) Chitosan (B) FA (C) FA-Chi conjugates

Table 3: Optimization of formulation variables based on particle size, PDI, and Dex-Cur % EE

Effect of different amounts of FA-Chi conjugates, with 10mg soya lecithin, 10mg Dex, 10mg Cur, and 10000 rpm					
Formulation	**FA-Chi conjugates (mg)**	**Particle size (nm)**	**PDI (%)**	**% EE (Dex)**	**% EE (Cur)**
F1	10	299.48±0.175	0.264±0.173	64.841±0.121	77.259±0.069
F2	50	345.00±3.605	0.231±0.230	67.485±0.206	83.176±0.294
F3	**100**	**411.67±3.055**	**0.150±0.152**	**80.147±0.020**	**96.676±0.093**
F4	200	543.00±3.000	0.224±0.152	91.792±0.287	99.609±0.040
Effect of different amounts of soya lecithin, with 100mg FA-Chi conjugates, 10 mg Dex, 10mg Cur, and 10000 rpm					
	Soya lecithin (mg)				
F5	**50**	**350.67±4.041**	**0.184±0.200**	**87.517±0.047**	**99.105±0.066**
F6	100	385.33±3.511	0.231±0.230	87.545±0.266	98.797±0.043
F7	200	420.33±1.527	0.256±0.400	96.960±0.260	91.825±0.108
Effect of different amounts of Dex and Cur, with 100mg FA-Chi conjugates, 50mg soya lecithin, and 10000 rpm					
	Dex (mg)	**Cur (mg)**			
F8	**50**	10	**371.67±3.055**	**0.129±0.100**	**96.457±0.178**	**98.539±0.005**
F9	100	10	402.67±3.214	0.213±0.208	77.473±0.293	97.930±0.048
F10	10	**50**	**438.67±1.527**	**0.259±0.700**	**86.257±0.282**	**97.807±0.003**
F11	10	100	510.67±2.516	0.207±0.264	78.545±0.254	97.971±0.004
Effect of different stabilizers, with 100mg FA-Chi conjugates, 50mg soya lecithin, 50 mg Dex, 50mg Cur, and 10000 rpm					
	Stabilizers				
F12	Poloxamer 188	4522.33±2.516	0.238±0.264	89.982±0.074	98.684±0.031
F13	**PVA (Cold)**	**796.67±4.725**	**0.219±0.400**	**89.293±0.078**	**98.702±0.025**
F14	Tween 80	4680.70±6.027	0.268±0.264	89.503±0.118	98.697±0.033

Table 4: Optimization of process variables based on particle size, PDI, and Dex-Cur % EE

Effect of diff. homogenization speed at 100mg FA-Chi conjugates, 50mg soya lecithin, 50mg Dex & Cur each, PVA(cold)					
Formulation	**RPM**	**Particle size (nm)**	**PDI (%)**	**% EE (Dex)**	**% EE (Cur)**
F15	7500	929.00±3.464	0.806±0.200	89.606±0.052	98.691±0.024
F16	**10000**	**284.33±4.041**	**0.192±0.200**	**89.503±0.118**	**98.681±0.029**
F17	12500	210.33±3.511	0.238±0.152	89.249±0.003	99.083±0.009
Effect of different ranges of amplitude (%) at 100mg FA-Chi conjugates, 50 mg soya lecithin, 50mg Dex, and Cur each, 10000 rpm, and PVA (cold)					
	Amplitude (%)				
F18	**40**	**857.00±4.582**	**0.264±0.400**	**89.960±0.064**	**99.289±0.016**
F19	60	1084.33±2.081	0.185±0.458	88.628±0.036	98.735±0.005

Effect of independent variables on % entrapment of Cur

The experimental and predicted responses for the % entrapment of Cur (Y2) of the developed formulation are mentioned in Table 5. Based on BBD, combinations of independent variables (i.e. X1, X2, and X3) were selected and their effective response for Y2 was expressed using the following quadratic equation:

$$\%\boldsymbol{Entrapment\ of\ Cur} = \mathbf{96.8142} + \mathbf{0.737375}.\boldsymbol{X1} + \mathbf{0.136}.\boldsymbol{X2} - \mathbf{0.30213}.\boldsymbol{X3} + \mathbf{0.33525}.\boldsymbol{X1}.\boldsymbol{X2} + \mathbf{0.181}.\boldsymbol{X1}.\boldsymbol{X3} - \mathbf{0.54575}.\boldsymbol{X2}.\boldsymbol{X3} - \mathbf{0.30735}.\boldsymbol{X1^2} + \mathbf{0.4964}.\boldsymbol{X2^2} - \mathbf{1.06035}.\boldsymbol{X3^2}$$

The above-mentioned quadratic equation represents the measurable impact on the % entrapment of Cur and their interactions (X1X2, X1X3, and X2X3) due to the selected independent variables combinations. The effect on the dependent variable, specifically the % entrapment of Cur (Y2), was assessed using the P-value and F-value. The BBD was implemented to plot the 3D response surface and identify these impacts on Y2. Moreover, ANOVA and R2 were used to assess the significance of the applied model, as shown in Table 6. The R2 was found to be 0.976586, the F-value was found to be 32.44, and the P-value was found to be less than 0.0001. The difference between the predicted and adjusted R2S was also found to be less than 0.2. All the values determined by the ANOVA indicate the model significance. All the results obtained for the % entrapment of Cur are represented in the form of 3D response curves as shown in Figure 7 (A), (B), and (C) [46].

Effect of independent variables on particle size

The experimental and predicted responses for the particle size (Y3) of the developed formulation are mentioned in Table 5. Based on BBD, combinations of independent variables (i.e. X1, X2, and X3) were selected and their effective response for Y3 was expressed using the following mathematical equation:

$$\boldsymbol{Particle\ Size}\ (\boldsymbol{nm}) = \mathbf{318.334} + \mathbf{67.405}.\boldsymbol{X1} - \mathbf{32.5475}.\boldsymbol{X2} - \mathbf{254.928}.\boldsymbol{X3} + \mathbf{12.315}.\boldsymbol{X1}.\boldsymbol{X2} - \mathbf{87.475}.\boldsymbol{X1}.\boldsymbol{X3} - \mathbf{0.17}.\boldsymbol{X2}.\boldsymbol{X3} - \mathbf{6.472}.\boldsymbol{X1} + \mathbf{10.948}.\boldsymbol{X2^2} + \mathbf{173.552}.\boldsymbol{X3^2}$$

The measurable impact of the independent variables (X1, X2, and X3) and their interactions (X1X2, X1X3, and X2X3) on particle size (Y3) can be detected using the equation above. The significance of the response can be described using the p-value (<0.05), as shown in Table 6. The nature and magnitude of the effect on the responses were determined from the signs and the resulting coefficient values. The positive sign on the coefficients of independent variables indicates the cordial effect, whereas the negative sign of the coefficient of independent variables indicates the divergent effect. The greater the value of a factor, the more substantial its effect on the response. To the BBD, the quadratic model was implemented. In this study, the R^2 and ANOVA were used to detect and verify the model's effectiveness. The R^2 value was 0.999, and the p-value was less than 0.0001, confirming the significance of the independent variables in predicting the response. The particle size results are presented as 3D response curves in Figures 8(A), (B), and (C). The difference between the adjusted R2 & predicted R2 is less than 0.2, indicating a good fit of the applied model. The model F value was found to be 2096278.44 [44,48].

Physical appearance, percentage yield, % EE, and % DL of optimized DCFLP nanoparticle formulation

The formulated nanoparticles exhibited a pale yellow color with uniform morphology & a high yield of 94.06 ± 0.419%. The % EE for Dex & Cur were 89.119 ± 0.087% and 98.272 ± 0.110 %, respectively. Drug loading % was 19.83 ± 0.201% for Dex and 21.87 ± 0.224% for Cur [47].

Particle size, PDI, and ζ analysis of optimized DCFLP nanoparticles formulation

After preparing blank & drug-loaded LPHNPs, their particle size, ζ potential & PDI were assessed. The blank FLP nanoparticles had a size of 210.51 ± 1.53 nm, while the DCFLP nanoparticles measured 287.8 ± 1.32 nm. The increased size of DCFLP nanoparticles is due to co-encapsulation of Dex-Cur & surface modification with FA-chitosan conjugates, which enhance site-specific targeting through the enhanced permeability & retention (EPR) effect. The ζ-potential values of FLP & DCFLP nanoparticles were found to be −20 mV and +5.4 mV, respectively. In general, absolute ζ potential values greater than ±30 mV indicate strong electrostatic repulsion & good colloidal stability, whereas values near neutrality (<±10 mV) indicate a higher risk of aggregation. Accordingly, the positive ζ potential of +5.4 mV for DCFLP alone would suggest limited electrostatic stabilization. Nevertheless, the stability of DCFLP nanoparticles is not solely governed by electrostatic repulsion. The formulation incorporates both lipids & chitosan, which provide complementary stabilization mechanisms. The cationic nature of chitosan facilitates drug–polymer interactions & imparts steric hindrance through its extended polymeric chains,

thereby minimizing aggregation. In parallel, the lipid matrix contributes hydrophobic interactions & structural integrity, further enhancing stability. PDI values of 0.81 & 0.25 for FLP & DCFLP, respectively. As per std. nanopharmaceutical formulation guidelines, a PDI value below 0.3 is generally considered acceptable & indicates a reasonably narrow size distribution with good stability. The optimized formulation shows a PDI of 0.25, which falls within this acceptable range & suggests moderate to good homogeneity as depicted in Figure 9 [48].

Table 5: Experimental and predicted responses of the formulation with its coded factors

Formulation code	Independent variables			Dependent variables					
	Coded Factors			Observed Response			Predicted Response		
	X1	X2	X3	Y3	Y1	Y2	Y3	Y1	Y2
1	100	10	10000	410.33±2.081	79.205±0.404	97.227±0.018	410.44	79.58	97.26
2	55	10	12500	280.67±3.214	83.553±0.153	96.334±0.225	280.63	83.24	96.35
3	10	10	10000	300.33±1.527	66.220±0.557	96.549±0.024	300.26	66.58	96.46
4	10	30	12500	250.33±3.055	75.169±0.464	94.166±0.189	250.55	75.11	94.22
5	55	30	10000	318.00±1.732	85.455±0.134	97.125±0.119	318.33	85.46	96.81
6	55	30	10000	318.00±1.732	87.426±0.235	96.580±0.031	318.33	85.46	96.81
7	55	30	10000	318.67±2.081	86.103±0.717	97.053±0.153	318.33	85.46	96.81
8	10	30	7500	318.00±3.511	72.103±0.952	95.126±0.225	318.33	72.17	95.19
9	10	50	10000	585.33±0.577	76.327±0.697	96.109±0.160	585.46	75.95	96.06
10	55	50	12500	210.67±2.516	88.332±0.101	95.556±0.067	210.54	88.76	95.53
11	100	30	12500	215.33±1.527	87.104±0.133	96.129±0.177	215.19	87.16	96.06
12	55	30	10000	210.33±1.527	84.233±0.071	96.559±0.010	210.41	85.46	96.81
13	100	30	7500	318.67±3.214	87.104±0.133	96.365±0.073	318.33	87.03	96.30
14	55	10	7500	895.33±2.00	77.964±0.181	95.853±0.288	895.22	77.53	95.87
15	55	30	10000	790.00±1.732	84.026±0.013	96.754±0.132	790.14	85.46	96.81
16	100	50	10000	318.00±3.605	90.235±0.105	98.128±0.270	318.33	89.86	98.21
17	55	50	7500	370.00±3.511	91.354±0.099	97.258±0.070	369.98	91.66	97.23
Optimized Formulation (D18)									
D18	88.27	50	10587.99	287.88±0.831	89.119±0.087	98.272±0.110	286.52	90.45	97.84

Table 6: Model fitting statistics and ANOVA for the responses

Response	Model fitting	R^2	Adjusted R^2	SD	Model F value	Model *p-value*	% CV
Y_1	Quadratic	1.13	7.84	764.0233	65.39	< 0.0001	1.37343
Y_2	Quadratic	0.976	0.946	0.21133	32.44	< 0.0001	0.219213
Y_3	Quadratic	1	0.999	0.195966	2096278.44	< 0.0001	0.048734

FTIR studies, DSC, and XRD studies of optimized DCFLP nanoparticle formulation

FTIR spectra demonstrate the presence of characteristic functional groups of Dex, Cur, and excipients (i.e., soya lecithin, chitosan, FA) in the formulation. A distinctive peak observed at approximately 1700–1710 cm^{-1} corresponds to the C=O stretching vibration of the carbonyl group in Dex. Additionally, clear absorption bands at 1635.16 cm^{-1} and 1623.49 cm^{-1} correspond to the C=O stretching of the ketone group in Cur. The FTIR spectra also displayed a prominent peak at around 2928 cm^{-1}, which is associated with the O–H stretching vibration of carboxylic acid groups in pure lecithin. Furthermore, a sharp band in the 1514–1520 cm^{-1} region corresponds to amide/amine functional groups, characteristic of chitosan in the formulation. Notably, the carbonyl stretching (C=O) peaks of both drugs, detected initially at 1715–1720 cm^{-1}, were shifted to 1700 cm^{-1} in the optimized formulation. This shift may be attributed to electrostatic interactions between chitosan & lipid molecules

(soya lecithin). Moreover, the observed changes in peak intensities further confirm the successful entrapment of the drugs within the carrier matrix through interactions with functional groups (Figure 10A) [41, 46].

DSC thermogram showed endothermic peaks at 179.39°C & 28.97°C for pure Dex & Cur, respectively. Phospholipid displayed a glass transition peak at 59.99°C. The physical mixture of FA-Chi conjugates, drugs & excipients retained individual drug peaks, indicating compatibility. In contrast, the nanoparticle formulation showed reduced peak intensities for both drugs, confirming their encapsulation within the nanoparticle matrix (Figure 10B). XRD analysis of pure Dex & Cur revealed sharp peaks at specific 2θ angles, confirming their crystalline nature. These peaks persisted in the physical mixture, suggesting no drug-excipient interactions. However, the nanoparticle formulation exhibited a broad, amorphous pattern, indicating drug encapsulation & alteration of the drug from its crystalline to amorphous form, which mainly enhances its apparent solubility & DR due to the higher free energy & the lack of a rigid lattice structure in the amorphous state. (Figure 10C) [49].

Transmission Electron Microscopy (TEM)

The morphological characteristics of the optimized DCFLP nanoparticles were confirmed by TEM, which confirms the spherical shape with a size distribution in the 100-200 nm range. TEM images, shown in Figure 11 (A), at scales of 100 nm & 200 nm, demonstrated the uniform spherical shape of the particles [35]. The TEM histogram was also depicted in Figure 11 (B), in which the diameters of more than 20 nanoparticles were measured from multiple TEM images. The histogram was plotted to represent the particle size distribution, with a mean particle size of 241.10 nm and a standard deviation of 89.55 nm. The histogram provides a clear quantitative representation of the nanoparticle size profile, complementing the TEM micrographs [37].

Folate content

The conjugation efficiency of folate to chitosan was 42.69%. The FA content obtained in conjugation with FA-chitosan was 78.19 ± 1.2%. It may be decreased due to the fabrication and purification process [34].

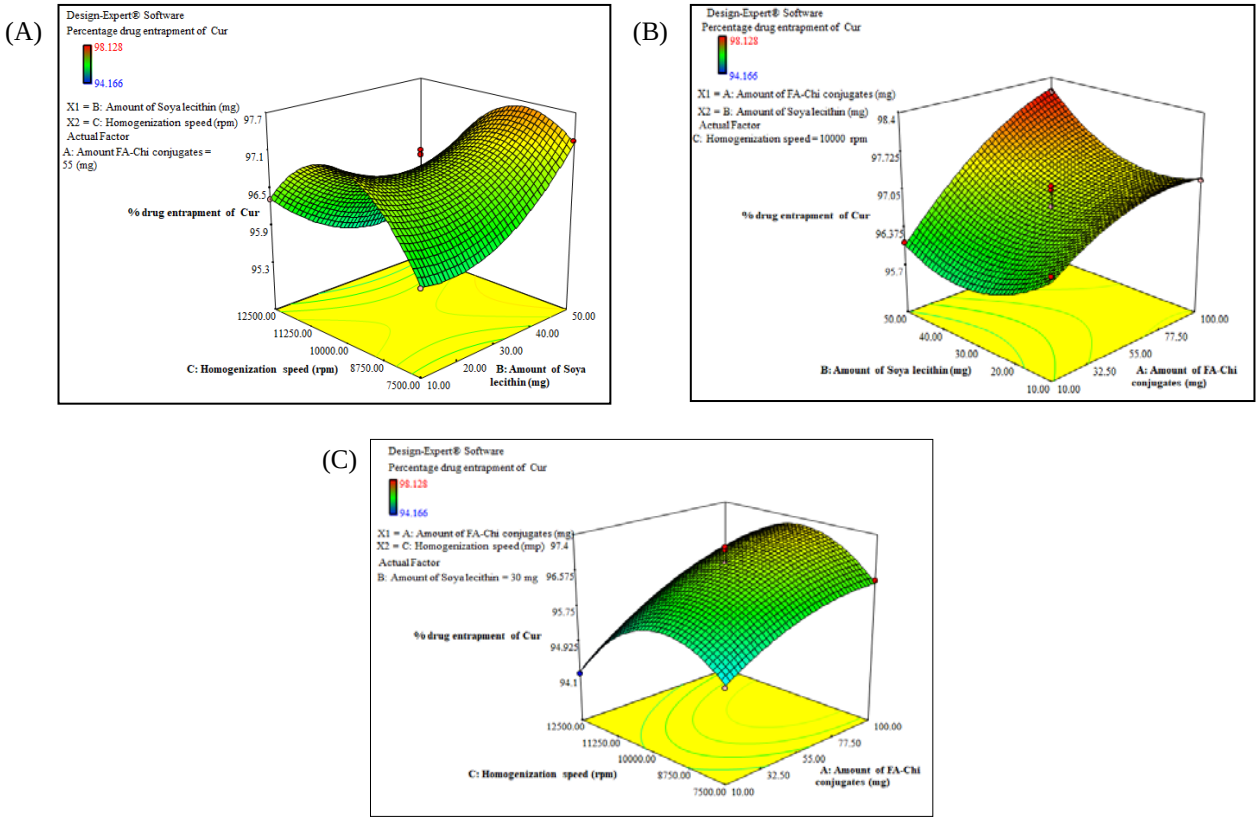

Figure 6: 3D Surface Response Graph of BBD showing the influence of, (A) Amount of FA-Chi conjugates (X_1), and Soya lecithin (X_2) on % entrapment of Dex (Y_1), (B) Amount of FA-Chi conjugates (X_1), and Homogenization Speed (X_3) on % entrapment of Dex (Y_1), (C) Amount of Soya lecithin (X_2), and Homogenization Speed (X_3) on % entrapment of Dex (Y_1)

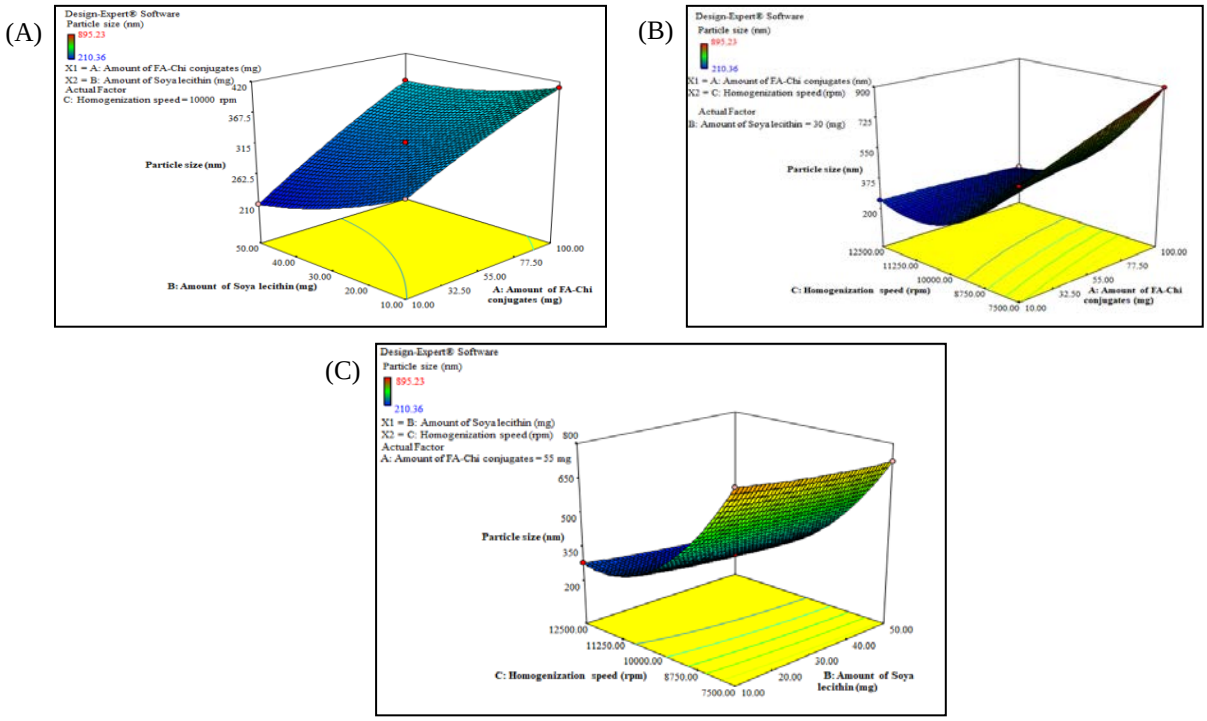

Figure 7: 3D Surface Response Graph of BBD showing the influence of, (A) Amount of Soya lecithin (X_2), and Homogenization speed (X_3) on % entrapment of Cur (Y_2), (B) Amount of FA-Chi conjugates (X_1), & Soya lecithin (X_2) on % entrapment of Cur (Y_2), (C) Amount of FA-Chi conjugates (X_1) & Homogenization speed (X_3) on % entrapment of Cur (Y_2)

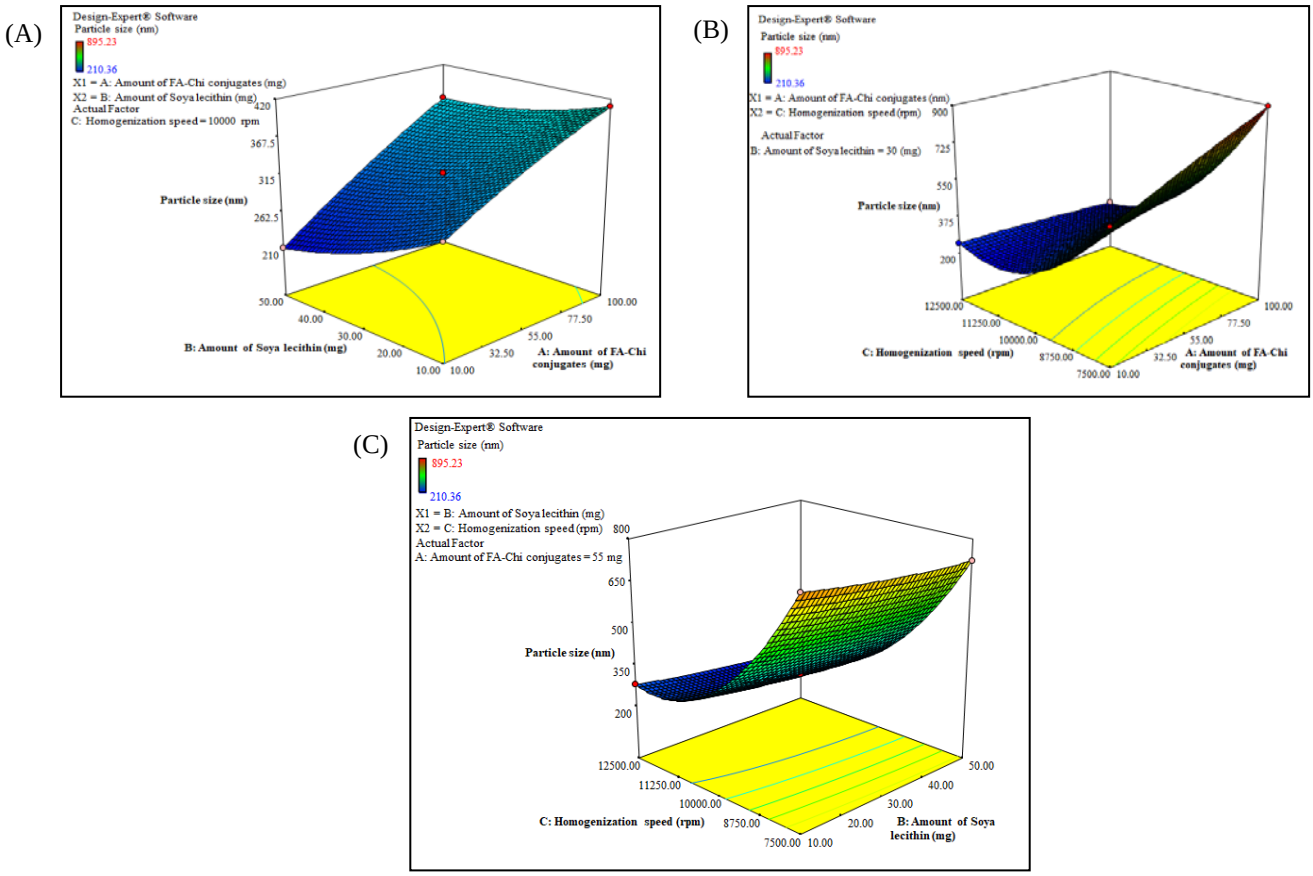

Figure 8: 3D Surface Response Graph of BBD showing the influence of, (A) Amount of FA-Chi conjugates (X_1), and Soya lecithin (X_2) on particle size (Y_3), (B) Amount of FA-Chi conjugates (X_1), and Homogenization speed (X_3) on particle size (Y_3), (C) Amount of Soya lecithin (X_2) and Homogenization speed (X_3) on particle size (Y_3)

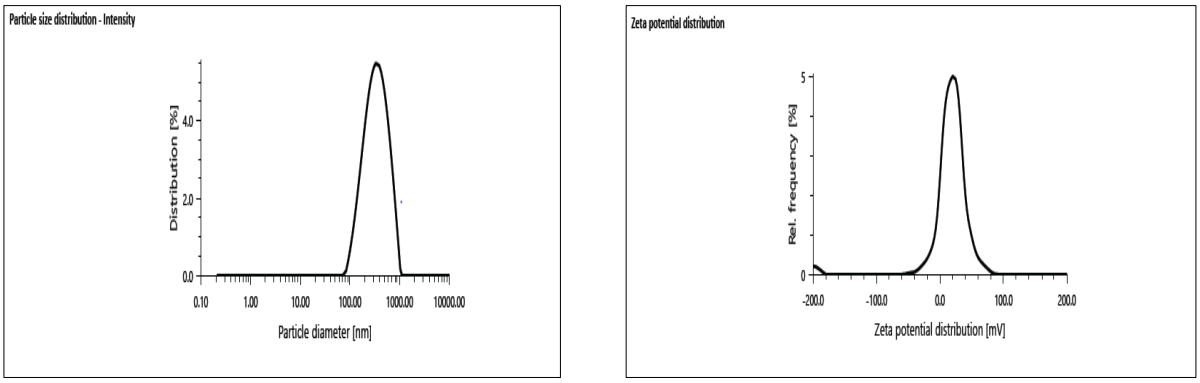

Figure 9: Particle size and zeta potential of optimized DCFLP nanoparticle formulation (±SD, n = 3); the significance levels were set at probabilities of * p < 0.05.

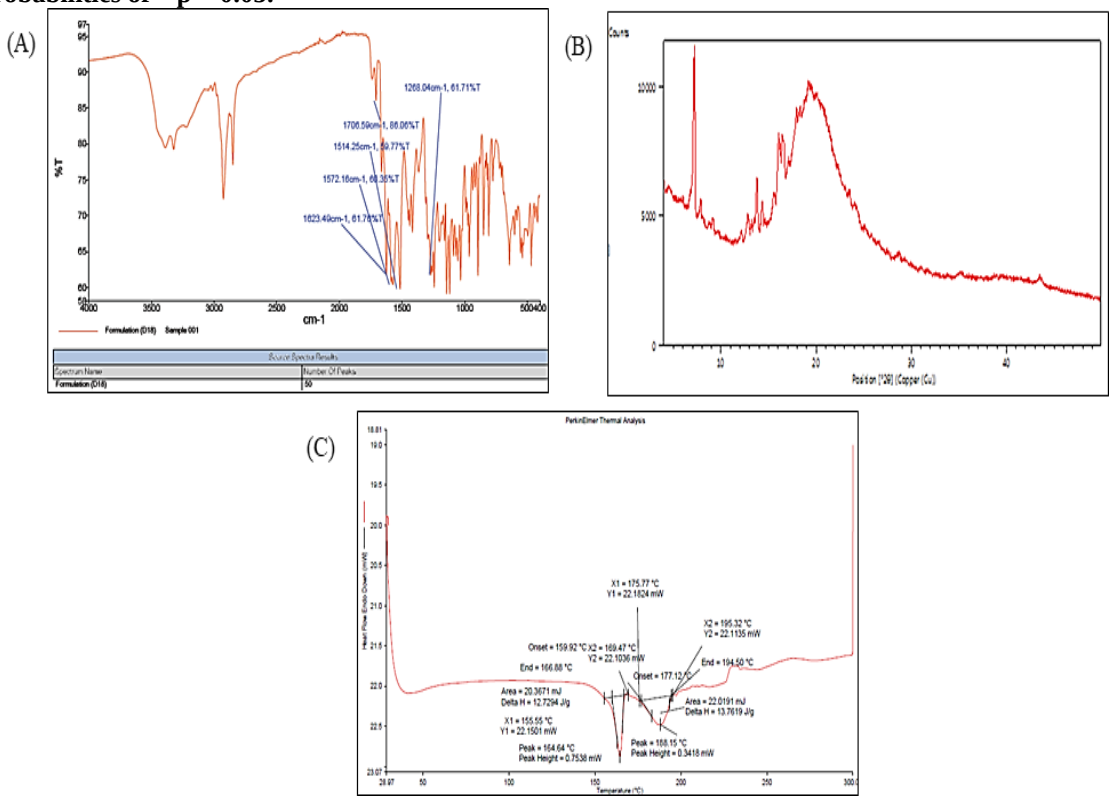

Figure 10: (A) FTIR Image (B) DSC thermograph (C) XRD of optimized DCFLP nanoparticle formulation

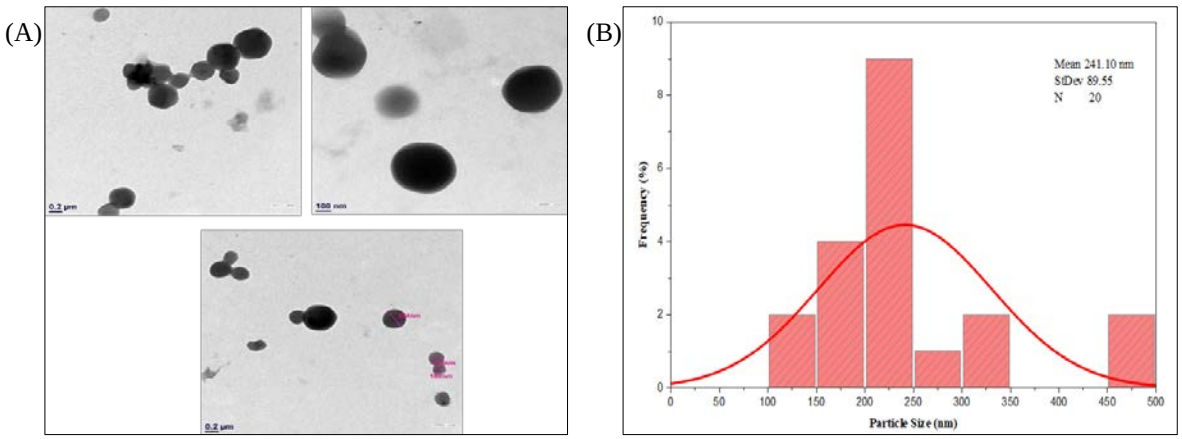

Figure 11: (A) TEM images showing the spherical morphology and nanoscale size distribution of optimized DCFLP nanoparticles, with sizes ranging from ~134 nm to 180 nm scale, (B) TEM-derived particle size distribution histogram of optimized DCFLP nanoparticles with average mean size 241.10 and SD 89.55.

***In-vitro* drug release studies of optimized formulation**

The in vitro drug release study of Dex from the developed formulation was evaluated in PBS at pH 7.4 under optimum conditions at 37°C (Figure 12). Initially, burst release was observed within the first 2–4 hours, from 19% to 27% and 18% to 31%, respectively. This initial rapid-release phase was subsequently followed by a sustained and controlled drug release over an extended period, likely due to the drug's entrapment within the nanoparticle core. Subsequently, a significant release was observed, corresponding to degradation of the nanoparticles to 75% and 80%, respectively, within 6-24 hours. After 24 hours, the formulation exhibited a controlled, slow-release profile. In contrast, pure Dex and Cur were rapidly released from the dialysis bag within 6 hours, with 99.43% and 99.50% release, respectively. The developed formulation showed 99.659±0.441% and 99.543±0.478% release of Dex and Cur, respectively, over 48 hours. Kantaria et al. also reported a biphasic release profile for dexamethasone-loaded pseudo-protein nanoparticles, consisting of a rapid initial burst release, followed by a prolonged, sustained release phase kinetics [40,42].

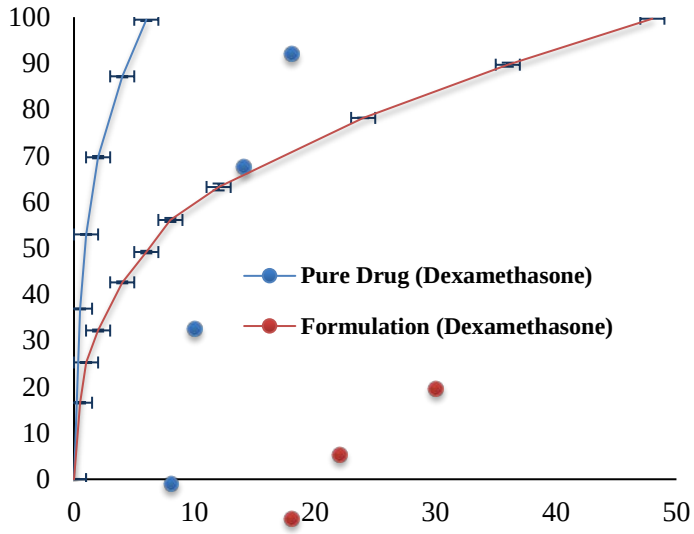

Figure 12: Percentage Drug Release Profile of Pure Dex and Dex from optimized DCFLP nanoparticle formulation

Due to Cur poor aqueous solubility, PBS, pH 7.4, was selected as the release medium under sink conditions at 37°C (Figure 13). Notably, approximately 99.51% of Cur was released within 6 hours. A burst release was observed within 2–4 hours, with the release escalating from 3.63% to 31.27%. The sustained release profile of the nanoparticles likely results from curcumin being embedded in their inner core. Subsequent release over 6–24 hours increased significantly, reaching 44.25% and 78.91%, possibly due to nanoparticle degradation. After 24 hours, the formulation exhibited a controlled, slow-release pattern, with 97.54% of Cur released at 48 hours [23,26].

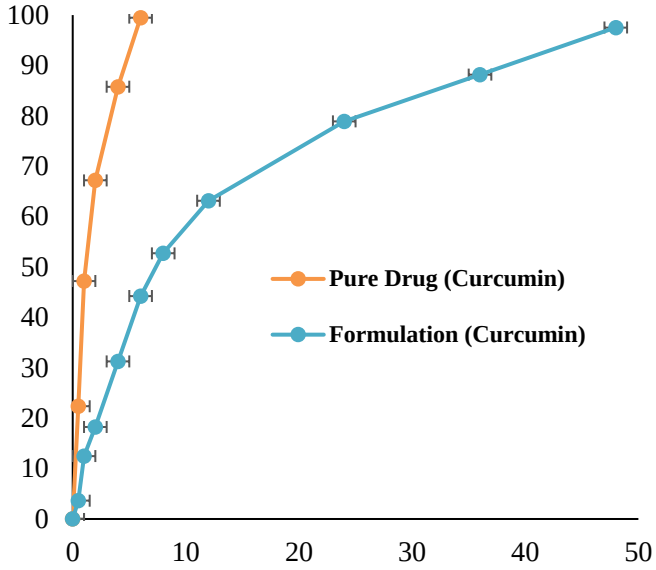

Figure 13: Percentage Drug Release Profile of Pure Cur and Cur from optimized DCFLP nanoparticle formulation

Drug release kinetic studies of Dex and Cur from the optimized formulation

Mathematical models can help to elucidate the kinetics of drug release. Drug release from the formulations was analyzed using zero-order, first-order, Higuchi, and Korsmeyer–Peppas models to determine the release mechanism. The released kinetics and corresponding determination coefficients (R^2) for both drugs (i.e., Dex and Cur) in the optimized formulations are presented in Figures 14(A) and 14(B). Among the models, the Higuchi model provided the best fit (R^2 = 0.966), indicating sustained, diffusion-controlled drug release from the lipid-polymer hybrid nanoparticle formulation [46].

Stability studies

Stability testing assesses the impact of temperature, humidity, and light on drug quality, providing insights into re-test intervals and shelf life. The physical stability of DCFLP was monitored for six months, assessing visual appearance, drug loading, and particle size under varying storage conditions: room temperature, refrigeration (4±2 °C), and protection from light using amber glass vials. The organoleptic characteristics, such as appearance, odor, and color, of the formulations were assessed under varying storage conditions. Results showed

consistent nanoparticle stability at room temperature and 4±2 °C over 180 days. No odor was detected, and the light-yellow color remained unchanged at 0, 30, 90, and 180 days, indicating sustained sensory stability suitable for long-term storage [40].

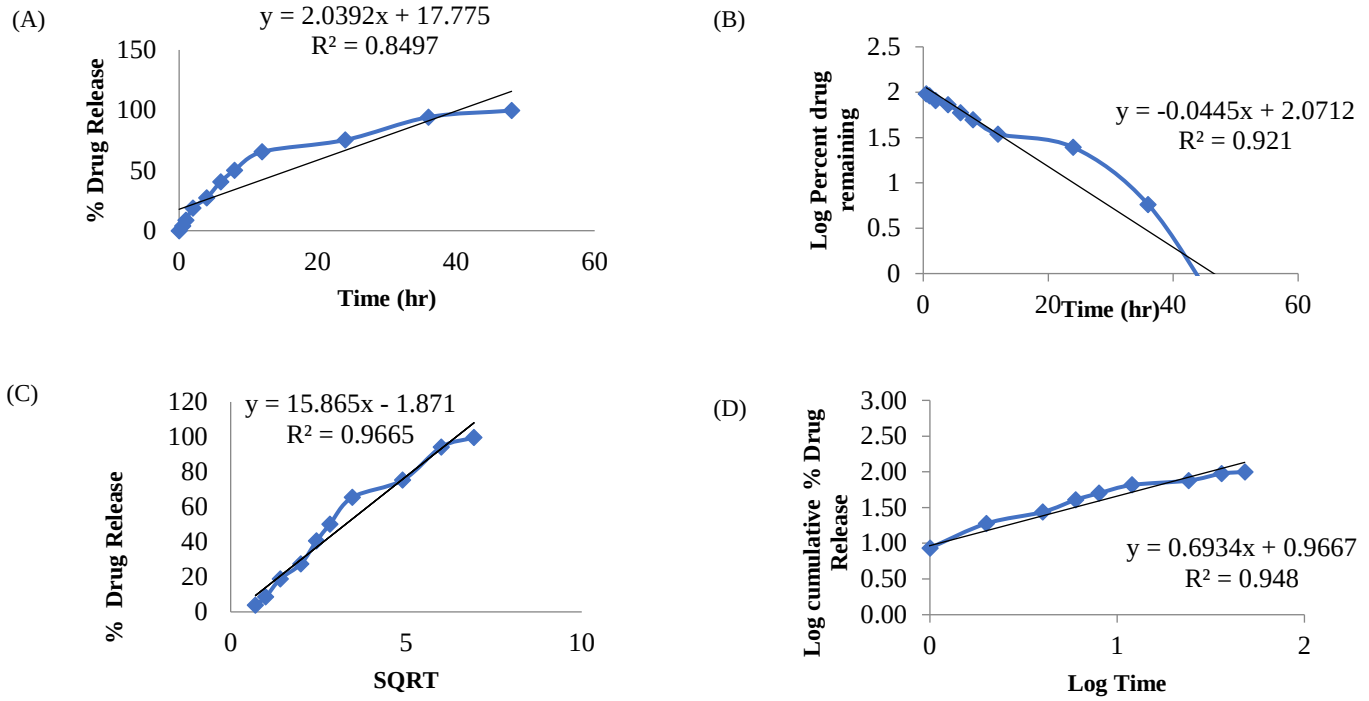

Figure 14A: Graph of optimized formulation (D18) for (A) Zero order, (B) First order, (C) Higuchi order, (D) Korsmeyer–Peppas order release kinetics of Dex.

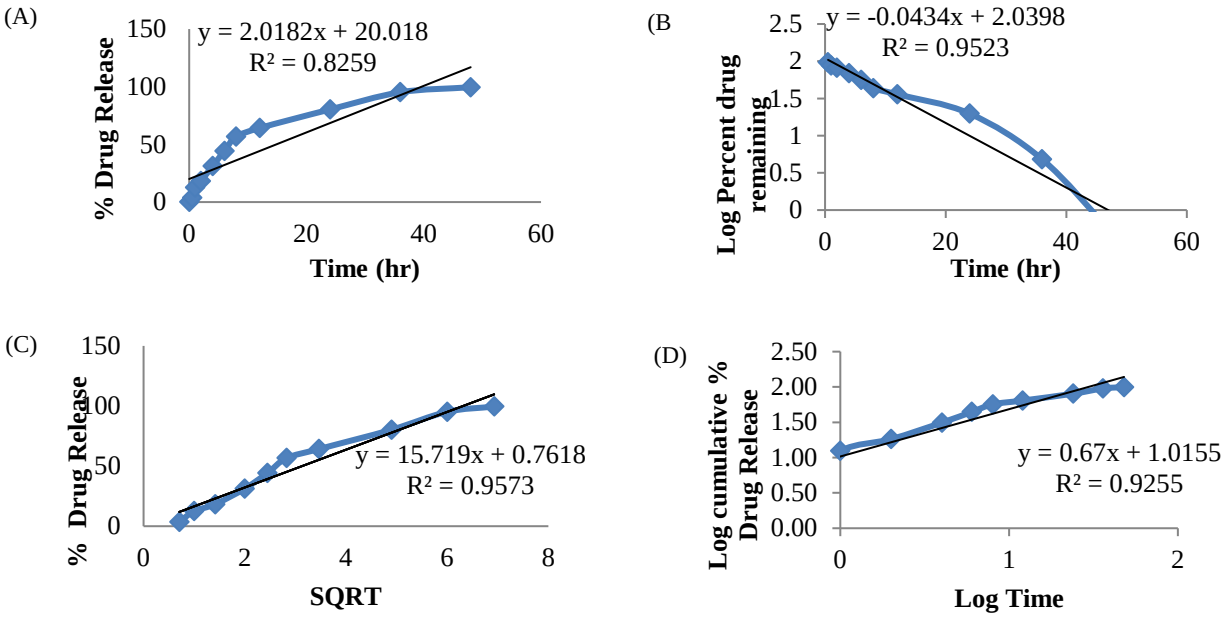

Figure 14B: Graph of optimized formulation (D18) for (A) Zero order, (B) First order, (C) Higuchi order, (D) Korsmeyer–Peppas order release kinetics of Cur.

% Drug Loading

The percentage drug loading (% DL) values for the nanoparticles show negligible variation over a 180-day storage period. Specifically, the drug loading of Dex and Cur remained stable under both room temperature (RT) and refrigerated conditions (4 ± 2°C). For Dex at 0 day, the % DL for the control and refrigerated samples were 22.309 ± 0.276% and 22.583 ± 0.371%, respectively. These values remained consistent at

22.653 ± 0.299% (RT) and 22.984 ± 0.609% (refrigerated) after 30 days, with slight increases observed at 90 days (22.720 ± 0.900% for RT and 22.884 ± 0.543% for refrigerated storage). By 180 days, the values slightly decreased to 22.07 ± 0.306% for RT and 22.03 ± 0.235% for refrigerated conditions. Similarly, at 0 days, the % DL was 24.782 ± 0.267% and 24.99 ± 0.29% for the control (RT) and refrigerated conditions (4 ± 2°C), respectively. Further, after 30 days, the samples were reanalyzed for % DL, resulting in slight decreases to 24.358 ± 0.315% and 24.744 ± 0.697% for RT and refrigerated conditions (4 ± 2°C), respectively. Then, after 90 days, these values change to 24.322 ± 0.482% and 24.582 ± 0.385%. By 180 days, values decreased further to 240129 ± 0.666% and 24.534 ± 0.517% for RT and refrigerated storage, respectively. These findings indicate the stability of drug loading over extended storage, underlining the robustness of the formulation. Along with this, the slight decrease in the drug loading values may be due to the drug leakage from the core of the nanoparticle (Figures 15 and 16).

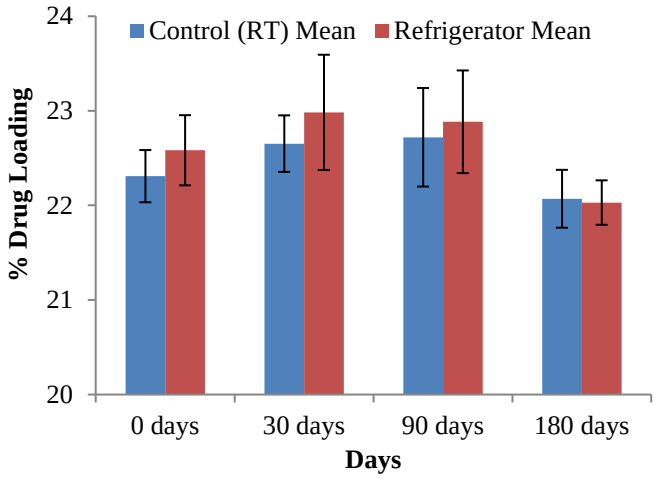

Figure 15: Drug loading efficiency of Dex in nanoparticles over a 180-day storage period.

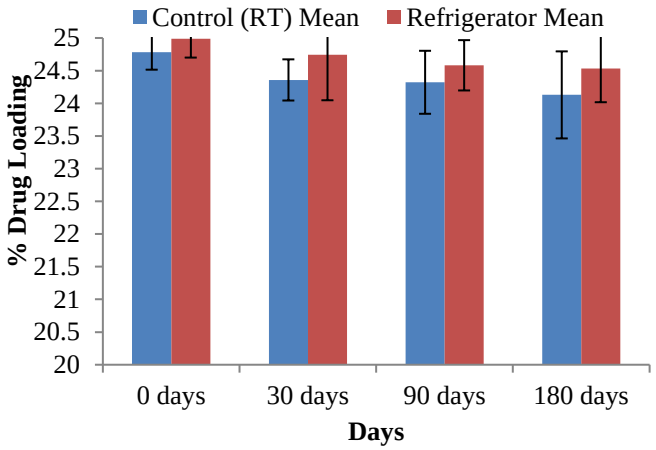

Figure 16: Drug loading efficiency of Cur in nanoparticles at 0 to 180 days of storage period

Particle Size

This study assessed the impact of storage parameters on nanoparticle size over 180 days. Initially, particle sizes were 287.167 ± 0.289 nm (RT) and 287.200 ± 0.265 nm (4 ± 2 °C). Measurements remained stable, with minor changes: 287.437 ± 0.378 nm (RT) and 287.623 ± 0.327 nm (refrigerated) at 30 days, 287.602 ± 0.088 nm and 287.567 ± 0.208 nm at 90 days, and 287.797 ± 0.382 nm and 287.684 ± 0.356 nm at 180 days. Temperature had a negligible influence on size stability (mean ± SD, n = 3) (Figure 17) [49].

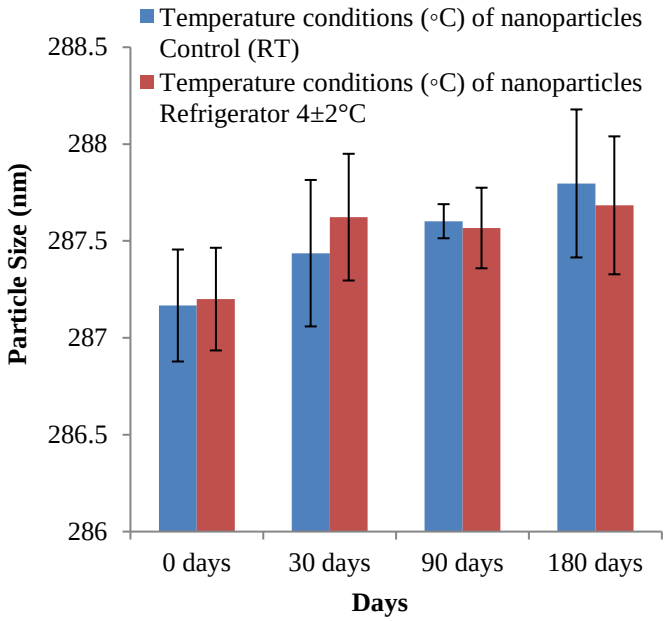

Figure 17: Particle size analyses of optimized nanoparticles over a 180-day storage period.

Cytotoxicity Study

Figure 18 showed cytotoxicity in RAW 264.7 macrophage cells at concentrations of the formulations ranging from 5 µg/mL to 100 µg/mL. The treatment with the pure drug showed a slight, concentration-dependent decrease in cell viability, retaining over 85% even at the highest dose (100 µg/mL), indicating low cytotoxicity. Moreover, the D18 formulation showed consistently higher cell viability (>95%) across all concentrations, suggesting excellent biocompatibility and a non-toxic nature of the nanoformulation. However, Formulation D18 co-treatment restored viability to a greater extent (to ~76% and ~88%, respectively, at 5 and 10 µg/mL), highlighting its enhanced protective effect compared with the pure drug. Statistical analysis revealed significant differences ($p < 0.05$ or $p < 0.01$) between the LPS alone group and the treated groups, confirming the anti-inflammatory efficacy of Formulation D18.

Intracellular Uptake Study

To evaluate intracellular uptake, optimized DCFLP nanoparticles (Formulation D18) were assessed using Rhodamine 123-loaded formulations in a comparative study against untreated controls. Fluorescence microscopy showed negligible uptake in control cells, whereas treated cells exhibited significantly enhanced fluorescence intensity at 5 µg and 10 µg, indicating efficient cellular internalization. The fluorescence signal was notably higher at 10 µg, reflecting a dose-dependent increase in uptake. These results suggest that the folate-targeted lipid-polymer hybrid system facilitates cellular entry via folate receptor-mediated endocytosis, supporting its potential for targeted intracellular drug delivery in inflammatory conditions such as rheumatoid arthritis (Figure 19) [39, 41].

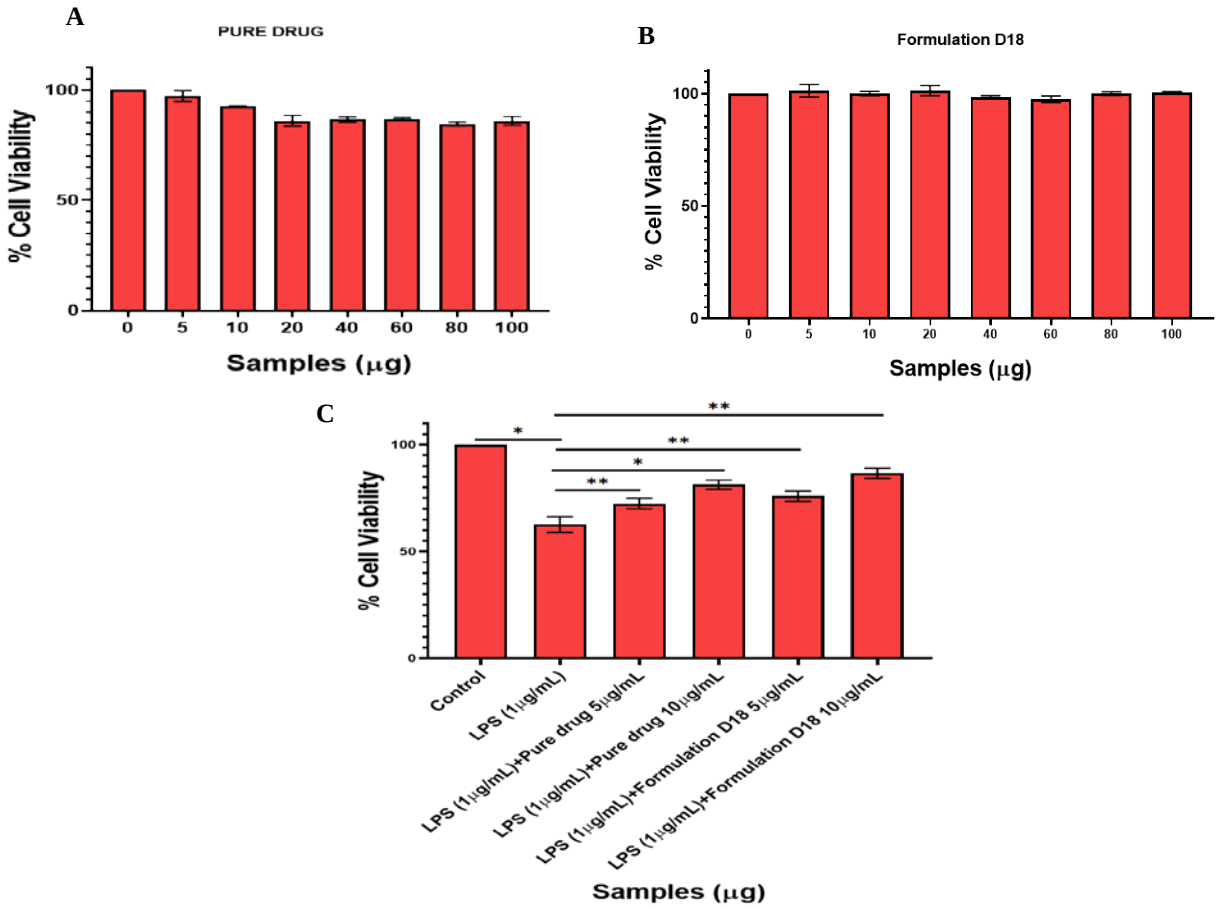

Figure 18: MTT assay showing cytotoxicity of (A) blank, (B) pure drug, and (C) DCFLP (D18) formulations, and their protective effects against LPS-induced toxicity in RAW 264.7 macrophage cells with significant improvement in cell viability (*p < 0.05, **p < 0.01).

CONCLUSION

This investigation demonstrated the design, optimization, and characterization of FTLPHNPs co-encapsulating Dex and Cur for the synergistic treatment of RA. The optimized formulation exhibited favorable physicochemical parameters, including a nano-scale particle size of 287.8 ± 1.32 nm, low PDI (0.25%), positive surface charge (+5.4 mV), and high entrapment efficiencies (Dex: 89.12 ± 0.087%, Cur: 98.27 ± 0.110%), corroborating the success of BBD-based optimization. These findings align with previous studies, which have shown improved encapsulation and stability in dual-loaded systems. TEM analysis confirmed DCFLP's spherical, uniform nano-scale structure, which enhances uptake via folate receptor-mediated endocytosis, consistent with the findings of Li et al. In vitro drug release studies showed a biphasic, diffusion-controlled pattern for both drugs, with the Higuchi model providing the best fit ($R^2 = 0.957$).

Encapsulation improved Cur's solubility and dexamethasone's specificity, thereby overcoming significant issues related to bioavailability and toxicity. ICH-guided stability tests confirmed minimal variation in particle size, drug content, and physical

attributes over 180 days, supporting the formulation's long-term stability and clinical potential. The biological efficacy of DCFLP was evident through enhanced cytotoxicity and cellular uptake, confirming targeted delivery to macrophages in RA. The combined delivery of Dex and Cur offers synergistic therapeutic benefits via anti-inflammatory and antioxidant mechanisms. Based on the results, it can be concluded that Dex- Cur-loaded FLPHNPs developed in the present study may be considered a potential anti-rheumatoid arthritis drug delivery system for effective RA treatment.

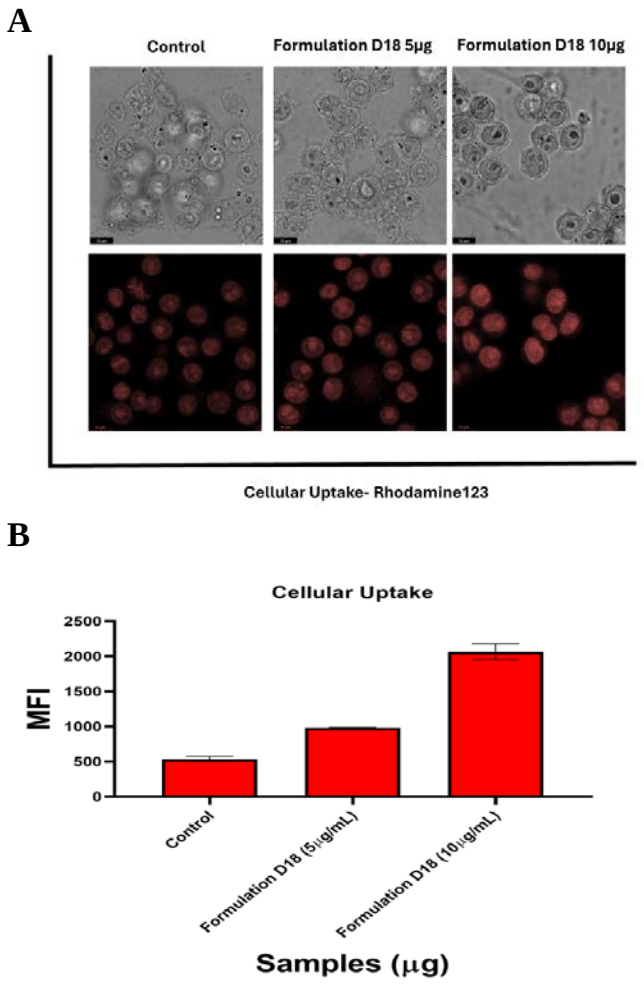

Figure 19: (A) Fluorescence microscopy images showing intracellular uptake of Rhodamine 123-loaded DCFLP nanoparticles (Formulation D18) at 5 µg/mL and 10 µg/mL concentrations compared to untreated control cells (B) Histogram representing normalized percentage intensity of green channels analyzed by ImageJ software Bar represents mean ± S.D (P < 0.05).

FINANCIAL ASSISTANCE
NIL

CONFLICT OF INTEREST
The authors declare no conflict of interest.

AUTHOR CONTRIBUTION
Ekta Panchal was involved in the study design and writing of the initial draft. Shiv Kumar Yadav reviewed the manuscript and edited the article. Neha Jain and Mahima Chauhan contributed to data interpretation and revised the manuscript. Archana Sharma contributed to the study's conception, supervision, and manuscript editing.

ABBREVIATIONS
RA: Rheumatoid Arthritis; LPHNPs: Lipid Polymer Hybrid Nanoparticles; Dex: Dexamethasone; Cur: Curcumin; BBD: Box-Behnken Design; DDS: Drug Delivery System; CIA: collagen-induced arthritis; FT-IR: Fourier transform-infrared spectroscopy; NMR: Nuclear Magnetic Resonance; TEM: Transmission Electron Microscopy; DCC: Dicyclohexylcarbodiimide; NHS: N-Hydroxysuccinimide; XRD: X-ray diffraction; 3D: Three Dimensional; RP-HPLC: Reverse Phase- High performance Liquid Chromatography; ANOVA: Analysis of variance

REFERENCES
[1] Xu Y, Zhao M, Cao J, Fang T, Zhang J, Zhen Y, Wu F, Yu X, Liu Y, Li J, Wang D. Applications and recent advances in transdermal drug delivery systems for the treatment of rheumatoid arthritis. *Acta Pharm. Sin. B*, **13**, 4417-41 (2023) https://doi.org/10.1016/j.apsb.2023.05.025.

[2] Cai Y, Zhang J, Liang J, Xiao M, Zhang G, Jing Z, Lv L, Nan K, Dang X. The Burden of Rheumatoid Arthritis: Findings from the 2019 Global Burden of Diseases Study and Forecasts for 2030 by Bayesian Age-Period-Cohort Analysis. *J. Clin. Med.*, **12**, 1291 (2023) https://doi.org/10.3390/jcm12041291.

[3] Singh S, Tiwary N, Sharma N, Behl T, Antil A, Anwer MK, Ramniwas S, Sachdeva M, Elossaily GM, Gulati M, Ohja S. Integrating Nanotechnological Advancements of Disease-Modifying Anti-Rheumatic Drugs into Rheumatoid Arthritis Management. *Pharmaceuticals*, **17**, 248 (2024) https://doi.org/10.3390/ph17020248.

[4] Khan S, Mohan K, Muzammil S, Alam MA, Khayyam KU. Current Prospects in Rheumatoid Arthritis: Pathophysiology, Genetics, and Treatments. *Recent Adv. Antiinfect. Drug Discov.*, **19**, 36-55 (2024) https://doi.org/10.2174/2772434418666230406083149.

[5] Li J, Li W, Zhuang L. Natural biomimetic nano-system for drug delivery in the treatment of rheumatoid arthritis: a literature

review of the last 5 years. *Front. Med.*, **11**, 1385123 (2024) https://doi.org/10.3389/fmed.2024.1385123.

[6] Bahmani A, Taghvaei A, Firozian F, Chehardoli G. Folic acid as an exploiter of natural endocytosis pathways in drug delivery. *Chem. Methodol*., **8**, 96-122 (2024) https://doi.org/10.48309/CHEMM.2024.430060.1746.

[7] Chandrupatla, D. M. S. H., Molthoff, C. F. M., Lammertsma, A. A., van der Laken, C. J., & Jansen, G. (2019). The folate receptor β as a macrophage-mediated imaging and therapeutic target in rheumatoid arthritis. *Drug Deliv. Transl. Res.*, **9**, 366–378 (2019) https://doi.org/10.1007/s13346-018-0589-2.

[8] Li C, Luo X, Qian C, Huang J, Yi X, Su H, Han Y. Folate receptor-mediated targeted therapy for rheumatoid arthritis by methotrexate-phospholipid complex nano-emulsions. *J. Drug Target.*, **31**, 402-410 (2023) https://doi.org/10.1080/1061186X.2023.2175832.

[9] Nasra S, Bhatia D, Kumar A. Targeted Macrophage Re-Programming: Synergistic Therapy With Methotrexate and RELA siRNA Folate-Liposome in RAW264.7 Cells and Arthritic Rats. *Adv. Healthc. Mater.*, **13**, 2400679 (2024) https://doi.org/10.1002/adhm.202400679.

[10] Guadarrama-Escobar OR, Serrano-Castañeda P, Anguiano-Almazán E, Vázquez-Durán A, Peña-Juárez MC, Vera-Graziano R, Morales-Florido MI, Rodriguez-Perez B, Rodriguez-Cruz IM, Miranda-Calderón JE, Escobar-Chávez JJ. Chitosan Nanoparticles as Oral Drug Carriers. *Int. J. Mol. Sci.*, **24**, 4289 (2023) https://doi.org/10.3390/ijms24054289.

[11] Jha R, Mayanovic RA. A Review of the Preparation, Characterization, and Applications of Chitosan Nanoparticles in Nanomedicine. *Nanomaterials*, **13**, 1302 (2023) https://doi.org/10.3390/nano13081302.

[12] Al-Nemrawi N, Wahsheh Y, Alzoubi KH. Transdermal Delivery of Methotrexate Loaded in Chitosan Nanoparticles to Treat Rheumatoid Arthritis. *Curr. Drug Deliv.*, **21**, 451-460 (2024) https://doi.org/10.2174/1567201820666230428124346.

[13] Naseer RD, Muhammad F, Aslam B, Faisal MN. Anti-arthritic effects of geranium essential oil loaded chitosan nanoparticles in Freund's complete adjuvant induced arthritic rats through down-regulation of inflammatory cytokines. *Inflammopharmacology*, **31**, 1893-1912 (2023) https://doi.org/10.1007/s10787-023-01233.

[14] Dong J, Zhou X, Li Q, Zheng R, Chen J, Liu Y, Tong X, Wan Z, Gong T. The Advances in Phospholipids-Based Phase Separation Gels for the Sustained Release of Peptides, Proteins, and Chemotherapeutics. *Pharmaceutics*, **16**, 875 (2024) https://doi.org/10.3390/pharmaceutics16070875.

[15] Jain S, Kumar M, Kumar P, Verma J, Rosenholm JM, Bansal KK, Vaidya A. Lipid–polymer hybrid nanosystems: a rational fusion for advanced therapeutic delivery. *J. Funct. Biomater.*, **14**, 437 (2023) https://doi.org/10.3390/jfb14090437.

[16] Zhang J, Yang J, Yu Z, Bai H, Wang Y, Wang R. DS-Modified Paeoniflorin pH-Responsive Lipid–Polymer Hybrid Nanoparticles for Targeted Macrophage Polarization in a Rat Model of Rheumatoid Arthritis. *International Journal of Nanomedicine*, **31**, 8967-92 (2025) https://doi.org/10.2147/IJN.S516434.

[17] Mrid RB, Bouchmaa N, Ainani H, El Fatimy R, Malka G, Mazini L. Anti-rheumatoid drugs advancements: New insights into the molecular treatment of rheumatoid arthritis. *Biomedicine & Pharmacotherapy*, **151**, 113126 (2022) https://doi.org/10.1016/j.biopha.2022.113126.

[18] Zhang Y, Zhou X, Wang Z, Wu M, Zhang W, Zhang Z, Sun X, Gong T. Dexamethasone Palmitate Encapsulated in Palmitic Acid Modified Human Serum Albumin Nanoparticles for the Treatment of Rheumatoid Arthritis. *J. Pharm. Sci.*, **113**, 2851-2860 (2024) https://doi.org/10.1016/j.xphs.2024.07.013.

[19] Kim SJ, Choi Y, Min KT, Hong S. Dexamethasone-Loaded Radially Mesoporous Silica Nanoparticles for Sustained Anti-Inflammatory Effects in Rheumatoid Arthritis. *Pharmaceutics*, **14**, 985 (2022) https://doi.org/10.3390/pharmaceutics14050985.

[20] Fuloria S, Mehta J, Chandel A, Sekar M, Rani NNIM, Begum MY, Subramaniyan V, Chidambaram K, Thangavelu L, Nordin R, Wu YS, Sathasivam KV, Lum PT, Meenakshi DU, Kumarasamy V, Azad AK, Fuloria NK. A Comprehensive Review on the Therapeutic Potential of *Curcuma longa* Linn. in Relation to its Major Active Constituent Curcumin. *Front Pharmacol.*, **13**, 820806 (2022) https://doi.org/10.3389/fphar.2022.820806.

[21] Asif HM, Zafar F, Ahmad K, Iqbal A, Shaheen G, Ansari KA, Rana S, Zahid R, Ghaffar S. Synthesis, characterization and evaluation of anti-arthritic and anti-inflammatory potential of curcumin loaded chitosan nanoparticles. *Sci. Rep.*, **13**, 10274 (2023) https://doi.org/10.1038/s41598-023-37152-7.

[22] Bideshki MV, Jourabchi-Ghadim N, Radkhah N, Behzadi M, Asemani S, Jamilian P, Zarezadeh M. The efficacy of curcumin in relieving osteoarthritis: A meta-analysis of meta-analyses. *Phytotherapy Research*., **38**, 2875-91 (2024) https://doi.org/10.1002/ptr.8153.

[23] Yan F, Li H, Zhong Z, Zhou M, Lin Y, Tang C, Li C. Co-delivery of prednisolone and curcumin in human serum albumin nanoparticles for effective treatment of rheumatoid arthritis. *International Journal of Nanomedicine*., **22**, 9113-25 (2019) https://doi.org/10.2147/IJN.S219413.

[24] Ponnusamy C, Krishnaswami V, Pandian S, Natesan S. In-vitro Drug Release and Ex-vivo Corneal Permeation of Dexamethasone and Curcumin Nanodispersions Using Facilitated Simultaneous RP-HPLC Technique. *Analytical Chemistry Letters*., **8**, 311- 20 (2018) https://doi.org/10.1080/22297928.2018.1445555.

[25] Patil N, Mahajan H. Development and validation of RP-HPLC method for simultaneous qualitative and quantitative estimation of curcumin and quercetin in bulk mixture. *Indian J Pharm Educ. Res.*, **56** ,247-54 (2022) https://doi.org/10.5530/ijper.56.1.29

[26] Aslam B, Hussain A, Faisal MN, Sindhu ZU, Khan RU, Alhidary IA, Naz S, Tufarelli V. Curcumin Co-Encapsulation Potentiates Anti-Arthritic Efficacy of Meloxicam Biodegradable Nanoparticles in Adjuvant-Induced Arthritis Animal Model. *Biomedicines.*, **11**, 2662 (2023) https://doi.org/10.3390/biomedicines11102662.

[27] Shahzad A, Arshad S, Zubair F, Shahzad S, Batool F, Fu Q. Development and Validation of Facile RP-HPLC Method for Simultaneous Determination of Timolol Maleate, Moxifloxacin Hydrochloride, Diclofenac Sodium and Dexamethasone in Plasma, Aqueous Humor and Pharmaceutical Products. *J Chromatogr.* Sci., **61**, 678-687 (2023) https://doi.org/10.1093/chromsci/bmac057.

[28] Ullah S, Azad AK, Nawaz A, Shah KU, Iqbal M, Albadrani GM, Al-Joufi FA, Sayed AA, Abdel-Daim MM. 5-fluorouracil-loaded folic-acid-fabricated chitosan nanoparticles for site-targeted drug delivery cargo. *Polymers.*, **14**, 2010 (2022) https://doi.org/10.3390/polym14102010.

[29] Kumbhar ST, Patil RY, Bhatia MS, Choudhari PB, Gaikwad VL. Synthesis and characterization of chitosan nanoparticles decorated with folate and loaded with dasatinib for targeting folate receptors in cancer cells. *OpenNano.*, **7**, 100043 (2022) https://doi.org/10.1016/j.onano.2022.100043.

[30] Khan MM, Madni A, Filipczak N, Pan J, Rehman M, Rai N, Attia SA, Torchilin VP. Folate targeted lipid chitosan hybrid nanoparticles for enhanced anti-tumor efficacy. *Nanomedicine: Nanotechnology, Biology and Medicine*., **28**, 102228 (2020) https://doi.org/10.1016/j.nano.2020.102228.

[31] San HH, Alcantara KP, Bulatao BP, Sorasitthiyanukarn FN, Nalinratana N, Suksamrarn A, Vajragupta O, Rojsitthisak P, Rojsitthisak P. Folic acid-grafted chitosan-alginate nanocapsules as effective targeted nanocarriers for delivery of turmeric oil for breast cancer therapy. *Pharmaceutics*, **15**, 110 (2022) https://doi.org/10.3390/pharmaceutics15010110.

[32] Murthy A, Ravi PR, Kathuria H, Vats R. Self-assembled lecithin-chitosan nanoparticles improve the oral bioavailability and alter the pharmacokinetics of raloxifene. *Int J Pharm.*, **588**, 119731 (2020) https://doi.org/10.1016/j.ijpharm.2020.119731.

[33] Shafique M, Ur Rehman M, Kamal Z, Alzhrani RM, Alshehri S, Alamri AH, Bakkari MA, Sabei FY, Safhi AY, Mohammed AM, Hamd MAE, Almawash S. Formulation development of lipid polymer hybrid nanoparticles of doxorubicin and its in-vitro, in-vivo and computational evaluation. *Front Pharmacol.*, **14**, 1025013 (2023) https://doi.org/10.3389/fphar.2023.1025013.

[34] Yadav B, Chauhan M, Dinkar R, Shekhar S, Singh RP. In silico modeling, development, characterization, in-vitro cytotoxicity, pharmacokinetic, and toxicological studies of folate-receptor targeted micelles containing cisplatin and upconversion nanoparticles for lung cancer therapy. *Materials Today Communications*, **39**, 109007 (2024) https://doi.org/10.1016/j.mtcomm.2024.109007.

[35] Li J, Zhang Z, Huang X. Tripterine and all-trans retinoic acid (ATRA) - loaded lipid-polymer hybrid nanoparticles for synergistic anti-arthritic therapy against inflammatory arthritis. *Artif Cells Nanomed Biotechnol.*, **49**, 575-585 (2021) https://doi.org/10.1080/21691401.2021.1964983.

[36] Aman RM, Zaghloul RA, Elsaed WM, Hashim IIA. In vitro-in vivo assessments of apocynin-hybrid nanoparticle-based gel as an effective nanophytomedicine for treatment of rheumatoid arthritis. *Drug Deliv Transl Res.*, **13**, 2903-2929 (2023) https://doi.org/10.1007/s13346-023-01360-5.

[37] Chauhan M, Singh RP, Sonali, Yadav B, Shekhar S, Kumar L, Mehata AK, Jhawat V, Dutt R, Garg V, Kailashiya V, Muthu MS. Dual-targeted transferrin and AS1411 aptamer conjugated micelles for improved therapeutic efficacy and imaging of brain cancer. *Colloids and Surf. B: Biointerfaces*, **231**, 113544 (2023) https://doi.org/10.1016/j.colsurfb.2023.113544.

[38] Negi S, Tandel N, Garg NK, Sharma P, Kumar R, Sharma P, Kumar R, Saini S, Sharma A, Tyagi RK. Co-delivery of aceclofenac and methotrexate nanoparticles presents an effective treatment for rheumatoid arthritis. *International Journal of Nanomedicine*, **31**, 2149-77 (2024) https://doi.org/10.2147/IJN.S439359.

[39] Mushtaq RY, Naveen NR, Rolla KJ, Al Shmrany H, Alshehri S, Salawi A, Kurakula M, Alghamdi MA, Rizg WY, Bakhaidar RB, Abualsunun WA. Design and evaluation of magnetic-targeted bilosomal gel for rheumatoid arthritis: flurbiprofen delivery using superparamagnetic iron oxide nanoparticles. *Frontiers in Pharmacology*, **15**, 1433734 (2024) https://doi.org/10.3389/fphar.2024.1433734.

[40] Zhao J, Zhang X, Sun X, Zhao M, Yu C, Lee RJ, Sun F, Zhou Y, Li Y, Teng L. Dual-functional lipid polymeric hybrid pH-responsive nanoparticles decorated with cell penetrating peptide and folate for therapy against rheumatoid arthritis. *Eur. J Pharm Biopharm.*, **130**, 39-47 (2018) https://doi.org/10.1016/j.ejpb.2018.06.020.

[41] Song Y, Yang P, Guo W, Lu P, Huang C, Cai Z, Jiang X, Yang G, Du Y, Zhao F. Supramolecular Hydrogel Dexamethasone–Diclofenac for the Treatment of Rheumatoid Arthritis. *Nanomaterials.*, **14**, 645 (2024) https://doi.org/10.3390/nano14070645.

[42] Al-Nemrawi N, Altawabeyeh R, Darweesh RS, Alnabulsi S. Coating methotrexate-PLGA nanoparticles with folic acid-chitosan conjugate for cancer targeting. *Pharmacia*, **71**, 1-9 (2024) https://doi.org/10.3897/pharmacia.71.e120072.

[43] Singh R, Jadhav K, Kamboj R, Malhotra H, Ray E, Jhilta A, Dhir V, Verma RK. Self-actuating inflammation responsive hydrogel microsphere formulation for controlled drug release in rheumatoid arthritis (RA): Animal trials and study in human fibroblast like synoviocytes (hFLS) of RA patients. *Biomaterials Advances.*, **160**, 213853 (2024) https://doi.org/10.1016/j.bioadv.2024.213853.

[44] Tahir N, Madni A, Balasubramanian V, Rehman M, Correia A, Kashif PM, Mäkilä E, Salonen J, Santos HA. Development and optimization of methotrexate-loaded lipid-polymer hybrid nanoparticles for controlled drug delivery applications. *International journal of pharmaceutics*, **533**, 156-68 (2017) https://doi.org/10.1016/j.ijpharm.2017.09.061.

[45] Bharti C, Nagaich U, Pandey J, Jain S, Jain N. Development of nitazoxanide-loaded colon-targeted formulation for intestinal parasitic infections: centre composite design-based optimization and characterization. *Future Journal of Pharmaceutical Sciences*, **6**, 119 (2020) https://doi.org/10.1186/s43094-020-00130-1.

[46] Zarei K, Jahanbakhshi M, Nahavandi R, Emadi R. Optimized co-delivery of curcumin and methylprednisolone using polyvinyl alcohol-coated CuO nanoparticles for synergistic rheumatoid arthritis treatment. *Heliyon*, **10** (2024) https://doi.org/10.1016/j.heliyon.2024.e40429.

[47] Zamanian MY, Zafari H, Osminina MK, Skakodub AA, Al-Aouadi RF, Golmohammadi M, Nikbakht N, Fatemi I. Improving dexamethasone drug loading and efficacy in treating rheumatoid arthritis via liposome: Focusing on inflammation and molecular mechanisms. *Animal Models and Experimental Medicine*, **8**, 5-19 (2025) https://doi.org/10.1002/ame2.12518.

[48] Bae Y, Zeb A, Choi HI, Ryu JS, Gul M, Noh HY, Cho J, Gil J, Shah FA, Chang SY, Bae ON. High payload dexamethasone palmitate-loaded solid lipid nanoparticles for enhanced anti-inflammatory effects in acute skin inflammation model. *Journal of Pharmaceutical Investigation*, **54**, 617-29 (2024) https://doi.org/10.1007/s40005-024-00674-x.

[49] Siddiqui B, ur Rehman A, Gul R, Chaudhery I, Shah KU, Ahmed N. Folate decorated chitosan-chondroitin sulfate nanoparticles loaded hydrogel for targeting macrophages against rheumatoid arthritis. *Carbohydrate polymers*, **327**, 121683 (2024) https://doi.org/10.1016/j.carbpol.2023.121683.